ATTACHMENT B: AREA OF REVIEW AND CORRECTIVE ACTION PLAN

Facility Information

Facility Name: FutureGen 2.0 Morgan County CO_2 Storage Site
IL-137-6A-0001 (Well #1)

Facility Contacts: Kenneth Humphreys, Chief Executive Officer,
FutureGen Industrial Alliance, Inc., Morgan County Office,
73 Central Park Plaza East, Jacksonville, IL 62650, 217-243-8215

Location of Injection Well: Morgan County, IL; 26−16N−9W; 39.80111ºN and 90.07491ºW

Computational Modeling

Model Name: STOMP-CO2 (Subsurface Transport Over Multiple Phases-CO2) simulator

Model Authors/Institution: White et al. 2013; White and Oostrom 2006; White and McGrail 2005/Pacific Northwest National Laboratory (PNNL)

Description of Model:

The simulations conducted for this investigation were executed using the STOMP-CO2 simulator (White et al. 2013; White and Oostrom 2006; White and Oostrom 2000). STOMP-CO2 was verified against other codes used for simulation of geologic disposal of CO_2 as part of the GeoSeq code intercomparison study (Pruess et al. 2002).

Partial differential conservation equations for fluid mass, energy, and salt mass compose the fundamental equations for STOMP-CO2. Coefficients within the fundamental equations are related to the primary variables through a set of constitutive relationships. The salt transport equations are solved simultaneously with the component mass and energy conservation equations. The solute and reactive species transport equations are solved sequentially after the coupled flow and transport equations. The fundamental coupled flow equations are solved using an integral volume finite-difference approach with the nonlinearities in the discretized equations resolved through Newton-Raphson iteration. The dominant nonlinear functions within the STOMP-CO2 simulator are the relative permeability-saturation-capillary pressure (k-s-p) relationships.

The STOMP-CO2 simulator allows the user to specify these relationships through a large variety of popular and classic functions. Two-phase (gas-aqueous) k-s-p relationships can be specified with hysteretic or nonhysteretic functions or nonhysteretic tabular data. Entrapment of CO_2 with imbibing water conditions can be modeled with the hysteretic two-phase k-s-p functions. Two-phase k-s-p relationships span both saturated and unsaturated conditions. The aqueous phase is assumed to never completely disappear through extensions to the s-p function below the residual

saturation and a vapor pressure lowering scheme. Supercritical CO_2 has the function of a gas in these two-phase k-s-p relationships.

For the range of temperature and pressure conditions present in deep saline reservoirs, four phases are possible: 1) water-rich liquid (aqueous), 2) CO_2-rich vapor (gas), 3) CO_2-rich liquid (liquid-CO_2), and 4) crystalline salt (precipitated salt). The equations of state express 1) the existence of phases given the temperature, pressure, and water, CO_2, and salt concentration; 2) the partitioning of components among existing phases; and 3) the density of the existing phases. Thermodynamic properties for CO_2 are computed via interpolation from a property data table stored in an external file. The property table was developed from the equation of state for CO_2 published by Span and Wagner (1996). Phase equilibria calculations in STOMP-CO2 use the formulations of Spycher et al. (2003) for temperatures below 100°C and Spycher and Pruess (2010) for temperatures above 100°C, with corrections for dissolved salt provided in Spycher and Pruess (2010). The Spycher formulations are based on the Redlich-Kwong equation of state with parameters fitted from published experimental data for CO_2-H2O systems. Additional details regarding the equations of state used in STOMP-CO2 can be found in the guide by White et al. (2013).

A well model is defined as a type of source term that extends over multiple grid cells, where the well diameter is smaller than the grid cell. A fully coupled well model in STOMP-CO2 was used to simulate the injection of supercritical CO_2 (scCO_2) under a specified mass injection rate, subject to a pressure limit. When the mass injection rate can be met without exceeding the specified pressure limit, the well is considered to be flow controlled. Conversely, when the mass injection rate cannot be met without exceeding the specified pressure limit, the well is considered to be pressure controlled and the mass injection rate is determined based on the injection pressure. The well model assumes a constant pressure gradient within the well and calculates the injection pressure at each cell in the well. The CO_2 injection rate is proportional to the pressure gradient between the well and surrounding formation in each grid cell. By fully integrating the well equations into the reservoir field equations, the numerical convergence of the nonlinear conservation and constitutive equations is greatly enhanced.

Model Inputs and Assumptions:

Conceptual Model

Site Stratigraphy

The regional geology of Illinois is well known from wells and borings drilled in conjunction with hydrocarbon exploration, aquifer development and use, and coal and commercial mineral exploration. Related data are largely publicly available through the Illinois State Geological Survey (ISGS)[1] and the U.S. Geological Survey.[2] In addition, the U.S. Department of Energy has sponsored a number of studies by the Midwest Geologic Sequestration Consortium[3] to evaluate subsurface strata in Illinois and adjacent states as possible targets for the containment of anthropogenic CO_2.

[1] http://www.isgs.uiuc.edu/
[2] http://www.usgs.gov/
[3] http://sequestration.org/

To support the evaluation of the Morgan County site as a potential carbon storage site, a deep stratigraphic well was drilled and extensively characterized. The FutureGen 2.0 stratigraphic well, located at longitude 90.05298W, latitude 39.80681N, is approximately 1.24 mi (2 km) northeast of the planned injection site. The stratigraphic well reached a total depth of 4,826 ft (1,471 m) below ground surface (bgs) within the Precambrian basement (Figure 1). The well penetrated 479 ft (146 m) of the Eau Claire Formation and 512 ft (156 m) of the Mount Simon Sandstone. The stratigraphic well was extensively characterized, sampled, and geophysically logged during drilling. A total of 177 ft of whole core were collected from the lower Eau Claire Formation and upper Mount Simon Sandstone and 34 ft were collected from lower Mount Simon Sandstone and Precambrian basement interval. In addition to whole drill core, a total of 130 side-wall core plugs were obtained from the combined interval of the Eau Claire Formation, Mount Simon Sandstone, and the Precambrian basement. In Figure 2, cored intervals are indicated with red bars; rotary side-wall core and core-plug locations are indicated to the left of the lithology panel. Standard gamma ray and resistivity curves are shown in the second panel.

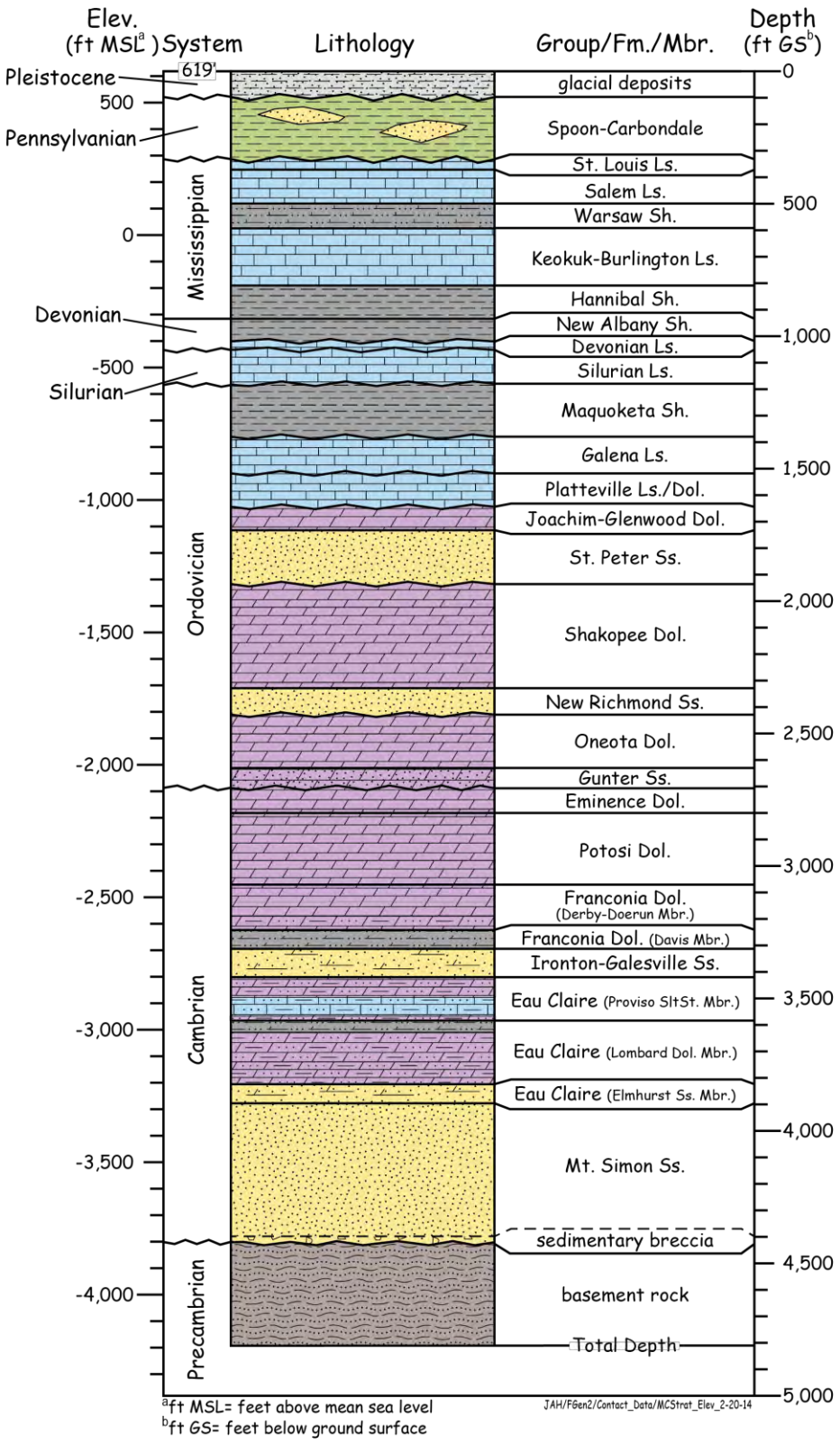

Figure 1. Stratigraphic Column of FutureGen 2.0 Stratigraphic Well

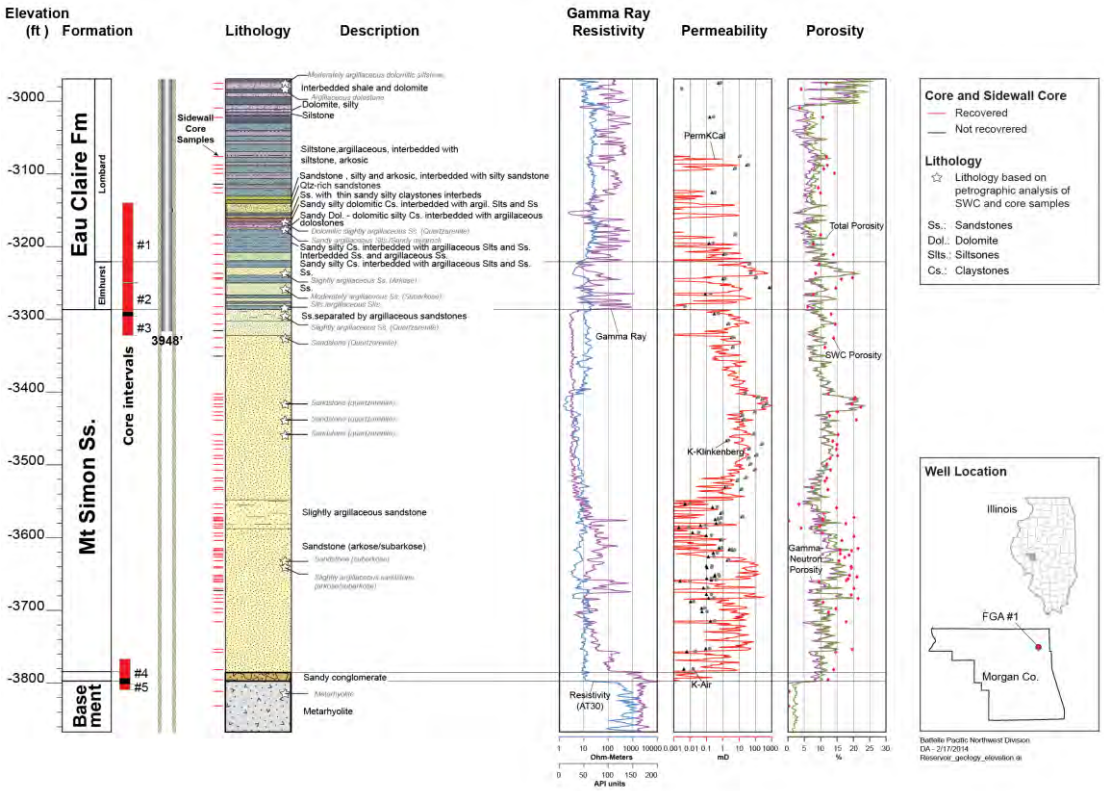

Figure 2. Lithology, Mineralogy, and Hydrologic Units of the Proposed Injection Zone (Mount Simon, Elmhurst and Lower Lombard member) and Lower Primary Confining Zone (Upper Lombard), as Encountered Within the Stratigraphic Well

Geologic Structures

Two orthogonal two-dimensional (2D) surface seismic lines, shown in Figure 3, were acquired along public roads near the site and processed in January and February 2011. Surface seismic data were acquired as single-component data. The seismic data are not of optimal quality due to loss of frequency and resolution below a two-way time depth of about 300 milliseconds (ms), approximately coincident with the top of the Galena limestone at a depth of 1,400 ft. However, they do not indicate the presence of obvious faults or large changes in thickness of the injection or confining zones. Both profiles indicate a thick sequence of Paleozoic-aged rocks with a contact between Precambrian and Mount Simon at 640 ms and a contact between Eau Claire and Mount Simon at 580 ms.

Some vertical disruptions, which extend far below the sedimentary basin, remain after reprocessing in 2012, but their regular spatial periodicity has a high probability of being an artifact during data acquisition and processing and is unlikely related to faults.

No discernable faults have been identified on the 2D data within the immediate area. A small growth fault that affects the Mount Simon and Eau Claire formations is interpreted in the eastern part of the L201 profile at an offset 28,000 ft. This growth fault is more than 1.5 miles away from the outermost edge of the CO_2 plume and does not extend far upward in the overburden. For these reasons, it is highly unlikely that it could affect the integrity of the injection zone.

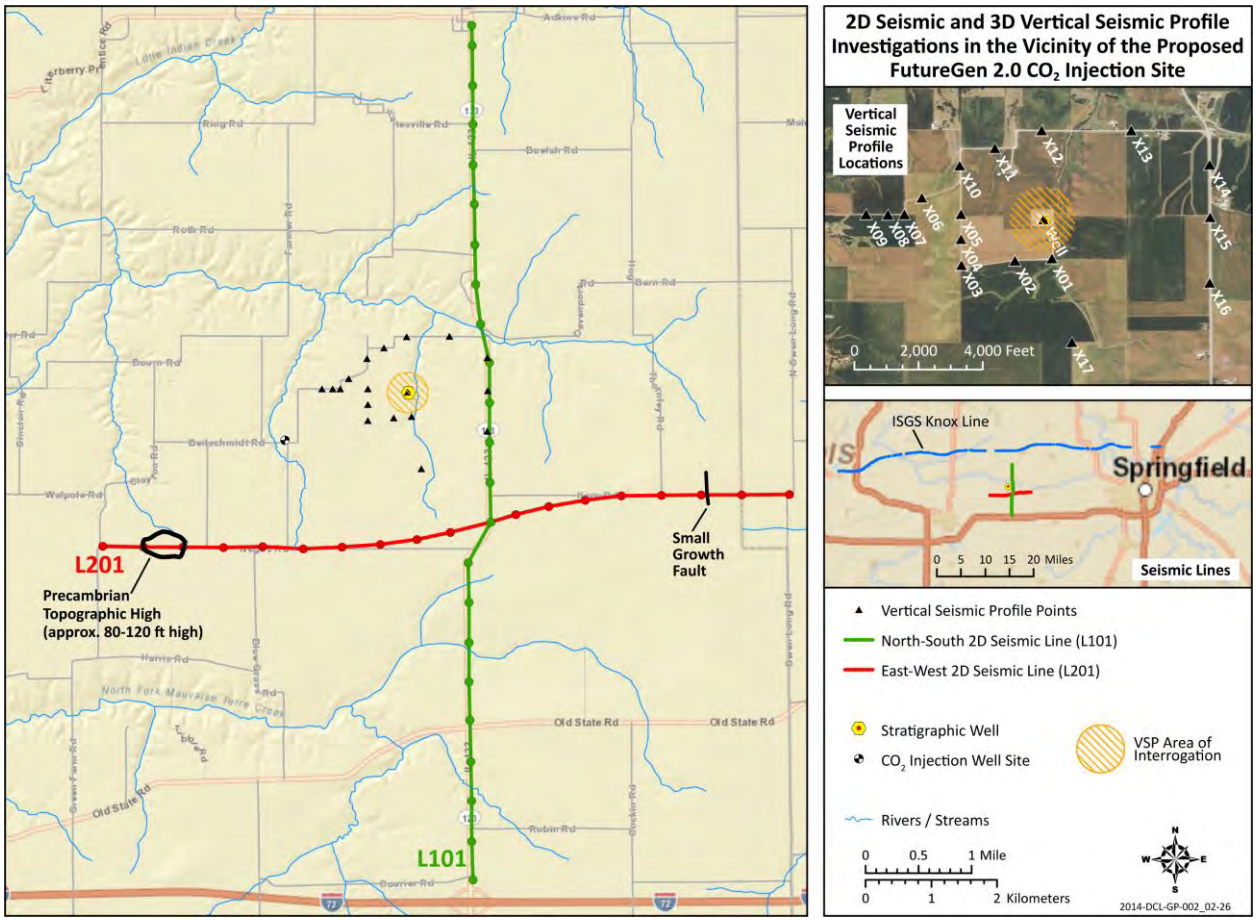

Figure 3. Locations of Two 2D Seismic Survey Lines, L101 and L201, Vertical Seismic Profile Locations, and the Knox Line Near the Proposed Morgan County CO_2 Storage Site

A three-component vertical seismic profiling (VSP) data set (Figure 3) was acquired in the FutureGen stratigraphic well in March 2013, and processed by Schlumberger Carbon Services. No discernable faults are present in the 15 short 2D seismic lines formed by the offset VSP locations. These lines represent a lateral interrogation extent of 800−1600 ft radially from the stratigraphic well. The high-resolution, low-noise VSP data also do not contain the vertical disruptions observed in the 2D surface seismic profiles (Hardage 2013[4]).

The ISGS recently shot a 120-mi long seismic reflection survey (the Knox Line) across central Illinois as part of a Department of Energy-sponsored research project to characterize rock units for geologic storage of CO_2. The continuous east-west line extends from Meredosia to southwestern Champaign County (Figure 3). FutureGen Industrial Alliance, Inc., (FutureGen Alliance) acquired these data from the ISGS with the intention of reprocessing the data, if needed, to identify regional faults that might impact the proposed FutureGen 2.0 Morgan County CO_2 Storage Site (FutureGen 2.0 Site). A review of the data by a geophysical expert on Illinois reflection seismic data[5], indicated that there was no discernable faulting west of Ashland,

[4] Bob Hardage. Personal Communication with Charlotte Sullivan, August 1, 2013.
[5] John McBride. Personal Communication with Charlotte Sullivan, October 29, 2013.

Illinois; and that current plans to reprocess the ISGS Knox line would not likely result in a greatly improved image.

The closest known earthquake to the FutureGen 2.0 Site (Intensity VII, magnitude 4.8 – non-instrumented record) occurred on July 19, 1909, approximately 28 mi (45 km) north of the site; it caused slight damage. Most of the events in Illinois occurred at depths greater than 1.9 mi (3 km).

Conceptual Model Domain

A stratigraphic conceptual model of the geologic layers from the Precambrian basement to ground surface was constructed using the EarthVision® software package. The geologic setting and site characterization data described in the Underground Injection Control (UIC) Permit Supporting Documentation and later in this section were the basis for the Morgan County CO_2 storage site computational model. Borehole data from the FutureGen 2.0 stratigraphic well and data from regional boreholes and published regional contour maps were used as input data (Figure 4, step 1). There is a regional dip of approximately 0.25 degrees in the east-southeast direction (Figure 4, step 2). To define the numerical model domain, an expanded 100- by 100-mi conceptual model was constructed to represent units below the Potosi dolomite interval, including the formations of Franconia, Ironton, Eau Claire (Proviso, Lombard, and Elmhurst), and Mount Simon. Each of these formation layers was further divided into multiple sub-layers based on the data from the stratigraphic well. The elevations of Franconia top, Mount Simon top, and Mount Simon Bottom were determined by EarthVision® based on borehole data and regional contour maps. The elevations of the interfaces between sub-layers were determined by the three bounding surfaces from EarthVision® and the stratigraphic well to make up the boundary-fitted stratigraphic layers of the computational model. The numerical model grid in the horizontal directions was designed to have constant grid spacing with higher resolution in the area influenced by the CO_2 injection (3-mi by 3-mi area), with increasingly larger grid spacing moving out toward the domain boundaries. The conceptual model hydrogeologic layers were defined for each stratigraphic layer based on zones of similar hydrologic properties. The hydrologic properties (permeability, porosity) were deduced from geophysical well logs and side-wall cores. The lithology, deduced from wireline logs and core data, was also used to subdivide each stratigraphic layer of the model. Based on these data, the Mount Simon Sandstone was subdivided into 17 layers, and the Elmhurst Sandstone (member of the Eau Claire Formation) was subdivided into 7 layers (Figure 4). The Lombard and Proviso members of the Eau Claire Formation were subdivided respectively into 14 and 5 layers. The Ironton Sandstone was divided into four layers, the Davis Dolomite into three layers, and the Franconia Formation into one layer. Some layers ("split" label in Figure 4, step 2) have similar properties but have been subdivided to maintain a reasonable thickness of layers within the injection zone as represented in the computational model. The thickness of the layers varies from 4 to 172 ft, with an average of 26 ft.

Based on knowledge of the regional and local geology, the Mount Simon Sandstone and the Elmhurst form the main part of the injection zone. However, the computational model results indicate that the Model Layer "Lombard 5" is the top unit containing a fraction of injected CO_2 during the 100-year simulation. Based on these results, the lower part of the Lombard (layers Lombard 1 to 5 of the Computational Model), is considered to be part of the injection zone

(Figure 4). The top of the injection zone is set at 3,785 ft bgs (-3,153 ft elevation MSL) in the stratigraphic well. The upper part of the Lombard and the Proviso members form the primary confining zone.

Figure 4, step 3, shows the numerical model grid for the entire 100- by 100-mi domain and also for the 3- by 3-mi area with higher grid resolution and uniform grid spacing of 200 ft by 200 ft. The model grid contains 125 nodes in the x-direction, 125 nodes in the y-direction, and 51 nodes in the z-direction for a total number of nodes equal to 796,875. The expanded geologic model was queried at the node locations of the numerical model to determine the elevation of each surface for the stratigraphic units at the numerical model grid cell centers (nodes) and cell edges. Then each of those layers was subdivided into the model layers by scaling the thickness to preserve the total thickness of each stratigraphic unit. Once the vertical layering was defined, material properties were mapped to each node in the model.

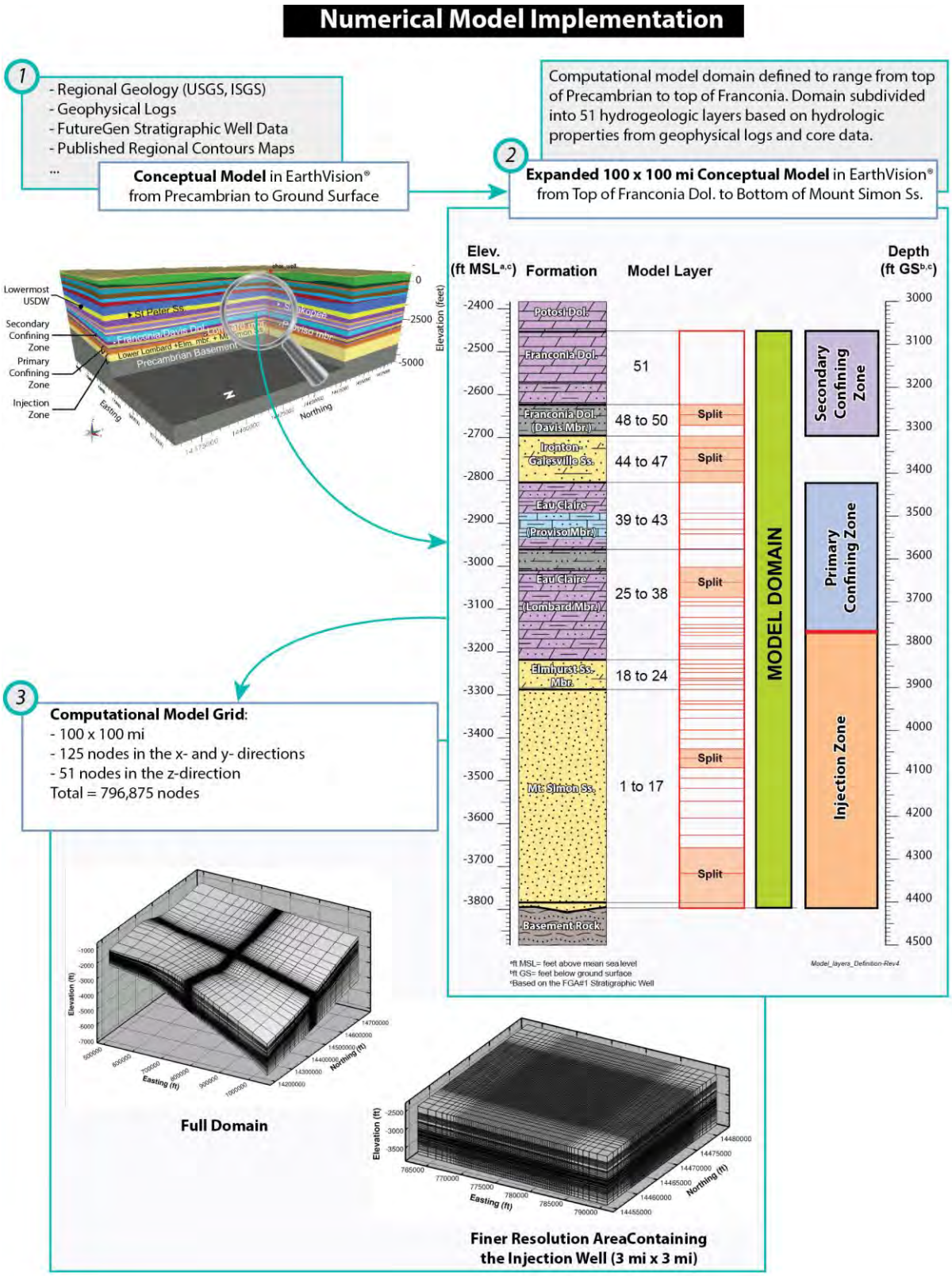

Figure 4. Implementation of the Numerical Model: From the Geological Conceptual Model to the Numerical Model

Processes Modeled

Physical processes modeled in the reservoir simulations included isothermal multi-fluid flow and transport for a number of components (e.g., water, salt, and CO_2) and phases (e.g., aqueous and gas). Isothermal conditions were modeled because it was assumed that the temperature of the injected CO_2 will be similar to the formation temperature. Formation salinity is considered because salt precipitation can occur near the injection well in higher permeability layers as the rock dries out during CO_2 injection. Porosity reduction due to salt precipitation is considered in the model. However, permeability reduction was not modeled because the salinity is relatively low in the injection formations at this site, resulting in low levels of salt precipitation.

Injected CO_2 partitions in the injection zone between the free (or mobile) gas, entrapped gas, and aqueous phases. Sequestering CO_2 in deep saline formations occurs through four mechanisms: 1) structural trapping; 2) aqueous dissolution; 3) hydraulic trapping; and 4) mineralization. Structural trapping is the long-term retention of the buoyant gas phase in the pore space of the permeable formation rock held beneath one or more impermeable or near impermeable confining zones. Aqueous dissolution occurs when CO_2 dissolves in the brine resulting in an aqueous-phase density greater than the ambient conditions. Hydraulic trapping is the pinch-off trapping of the gas phase in pores as the brine re-enters pore spaces previously occupied by the gas phase. Generally, hydraulic trapping only occurs upon the cessation of CO_2 injection. Mineralization is the chemical reaction that transforms formation minerals to carbonate minerals. In the Mount Simon Sandstone, the most likely precipitation reaction is the formation of iron carbonate precipitates. A likely reaction between CO_2 and shale is the dewatering of clays. Laboratory investigations are currently quantifying the importance of these reactions at the Morgan County CO_2 storage site. Based on its experiments, the FutureGen Alliance expects to see a small mass of precipitates (KCl, NaCl) forming near the injection well from the $scCO_2$ displacement of water, and does not expect to see the formation of any significant carbonate precipitates in the year (or years) time scale. Iron does precipitate, but concentrations are too low (<0.6 mmol/L) relative to carbonate mass to be a precipitate issue. Simulations by others (White et al. 2005) of $scCO_2$ injection in a similar sandstone (also containing iron oxides) shows that over significantly longer time scales (1000+ years), alumino silicate dissolution and alumino silicate precipitation incorporating significant carbonate (dawsonite) is predicted, as well as precipitation of some calcite. That predicted mineral trapping did permanently sequester 21 percent of the carbonate mass, thus decreasing $scCO_2$ transport risk. Therefore, the simulations described here did not include mineralization reactions. However, the STOMP-CO2 simulator does account for precipitation of salt during CO_2 injection. The CO_2 stream provided by the plant to the storage site is no less than 97 percent dry basis CO_2. Because the amount of impurities is small, for the purposes of modeling the CO_2 injection and redistribution for this project, it was assumed that the injectate was pure CO_2.

Rock Properties

Intrinsic Permeability

Site Characterization Data

Permeability in the sandstones, as measured in rotary side-wall cores and plugs from whole core, appears to be dominantly related to grain size and abundance of clay. In Figure 2, ELAN (Elemental Log Analysis)-calculated permeability (red curve) is in the third panel, along with two different lab measurements of permeability for each rotary side-wall core. Horizontal permeability (K_h) data in the stratigraphic well outnumber vertical permeability (K_v) data, because K_v could not be determined from rotary side-wall cores. However, K_v/K_h ratios were successfully determined for 20 vertical/horizontal siliciclastic core-plug pairs cut from intervals of whole core. Within the Mount Simon Sandstone, the horizontal permeabilities of the lower Mount Simon alluvial fan lithofacies range from 0.005 to 0.006 mD and average ratios of vertical to horizontal permeabilities range from 0.635 to 0.722 (at the 4,304 to 4,374 ft bgs depth or the elevation of -3,685 to -3,755 ft, Figure 2). Horizontal core-plug permeabilities range from 0.032 to 2.34 mD at the 3,838 to 3,904 ft bgs depth (elevation of -3,219 to -3,285 ft); K_v/K_h ratios for these same samples range from 0.081 to 0.833.

The computed lithology track for the primary confining zone indicates the upward decrease in quartz silt and increase in carbonate in the Proviso member, along with a decrease in permeability. The permeabilities of the rotary side-wall cores in the Proviso range from 0.000005 mD to 1 mD. Permeabilities in the Lombard member range from 0.001 mD to 28 mD, reflecting the greater abundance of siltstone in this interval, particularly in the lowermost part of the member. Whole core plugs and associated vertical permeabilities are available only from the lowermost part of the Lombard. Thin (few inches/centimeters), high-permeability sandstone streaks resemble the underlying Elmhurst; low-permeability siltstone and mudstone lithofacies have vertical permeabilities of 0.0004 to 0.465 mD, and K_v/K_h ratios of <0.0001 to 0.17.
The ELAN geophysical logs indicated permeabilities are generally less than the wireline tool limit of 0.01 mD throughout the secondary confining zone. Two rotary side-wall cores were taken from the Franconia, and three side-wall cores were cut in the Davis member. Laboratory-measured rotary side-wall core (horizontal) permeabilities are very low (0.000005 to 0.001 mD). The permeabilities of the two Franconia samples were measured with a special pulse decay permeameter; the sample from 3,140 ft bgs (-2521 ft elevation) has a permeability less than the lower instrument limit of 0.000005 mD. Vertical core plugs are required for directly determining vertical permeability and there are no data from the stratigraphic well for vertical permeability or for determining vertical permeability anisotropy in the secondary confining zone. However, K_v/K_h ratios of 0.007 have been reported elsewhere for Paleozoic carbonate mudstones (Saller et al. 2004).

Model Parameters

Intrinsic permeability data sources for the FutureGen 2.0 stratigraphic well include computed geophysical wireline surveys (CMR and ELAN logs), and where available, laboratory measurements of rotary side-wall cores (SWC), core plugs from the whole core intervals, hydrologic tests (including wireline [MDT]), and packer tests. For the Mount Simon and Elmhurst Sandstones model layers (3,838 to 4,418 ft bgs depth or elevation of -3219 to -3799 ft at the stratigraphic well), wireline ELAN permeability model permKCal produced by Schlumberger (red curve on Figure 2) was used. This model, calibrated by rotary side-wall and core-plug permeabilities, provides a continuous permeability estimate over the entire injection zone. This calibrated permeability response was then slightly adjusted, or scaled, to match the composite results obtained from the hydrologic packer tests over uncased intervals. For injection zone model layers within the cased well portion of the model, no hydrologic test data are available, and core-calibrated ELAN log response was used directly in assigning average model layer permeabilities.

The hydraulic packer tests were conducted in two zones of the Mount Simon portion of the injection zone. The Upper Zone (3,934 ft to 4,180 ft bgs depth or -3,315 to -3,561 ft elevation) equates to layers 6 through 17 of the model, while the Lower Zone (4,186 ft to 4,498 ft bgs depth or -3,567 to -3,879 ft elevation) equates to layers 1 through 5. The most recent ELAN-based permeability-thickness product values are 9,524 mD-ft for the 246-ft-thick section of the upper Mount Simon corresponding to the Upper Zone and 3,139 mD-ft for the 312-ft-thick section of the lower Mount Simon corresponding to the Lower Zone. The total permeability-thickness product for the open borehole Mount Simon is 12,663 mD-ft, based on the ELAN logs. Results of the field hydraulic tests suggest that the upper Mount Simon permeability-thickness product is 9,040 mD-ft and the lower Mount Simon interval permeability-thickness product is 775 mD-ft. By simple direct comparison, the packer test for the upper Mount Simon is nearly equivalent (~95 percent) to the ELAN-predicted value, while the lower Mount Simon represents only ~25 percent of the ELAN-predicted value.

Because no hydrologic test has been conducted in the Elmhurst Sandstone interval of the injection zone, a conservative scaling factor of 1 has been assigned to this interval, based on ELAN PermKCal data (The permeabilities used for this formation were the ELAN PermKCal values without applying a scaling factor). The sources of data for confining zones (Franconia to Upper part of the Lombard Formations) and the Upper part of the Injection zone (Lower part of the Lombard) are similar to those for the injection zone, with the exception that no hydrologic or MDT test data are available. ELAN log-derived permeabilities are unreliable below about 0.01 mD (personal communication from Bob Butsch, Schlumberger, 2012). Because the average log-derived permeabilities (permKCal wireline from ELAN log) for most of the confining zone layers are at or below 0.01 mD, an alternate approach was applied. For each model layer the core data were reviewed, and a simple average of the available horizontal Klinkenburg permeabilities was then calculated for each layer. Core samples that were noted as having potential cracks and/or were very small were eliminated if the results appeared to be unreasonable based on the sampled lithology. If no core samples were available and the arithmetic mean of the PermKCal was below 0.01 mD, a default value of 0.01 mD was applied (Lombard9 is the only layer with a 0.01-mD default value). Because the sandstone intervals of the Ironton-Galesville Sandstone have higher permeabilities that are similar in magnitude to the modeled injection zone layers, the Ironton-Galesville Sandstone model layer permeabilities were derived from the arithmetic mean

of the PermKCal permeability curve. Because no hydraulic test has been conducted in the primary confining zone and the Upper part of the injection zone (Elmhurst Sandstone layers and lower part of the Lombard – Lombard 1 to Lombard 5), the scaling factor was assigned to be 100 percent in this interval and the overburden formations. Figure 5 shows the depth profile of the horizontal permeability assigned to each layer of the model and actual values assigned are listed in Table 1. Figure 6 shows the distribution of horizontal and vertical permeability as it was assigned to the numerical model layers.

Because the anisotropy of the model layers is not likely to be represented by the sparse data from the stratigraphic well, the lithology-specific permeability anisotropy averages from literature studies representing larger sample sizes were used for the model layers (Table 2 and Table 3).

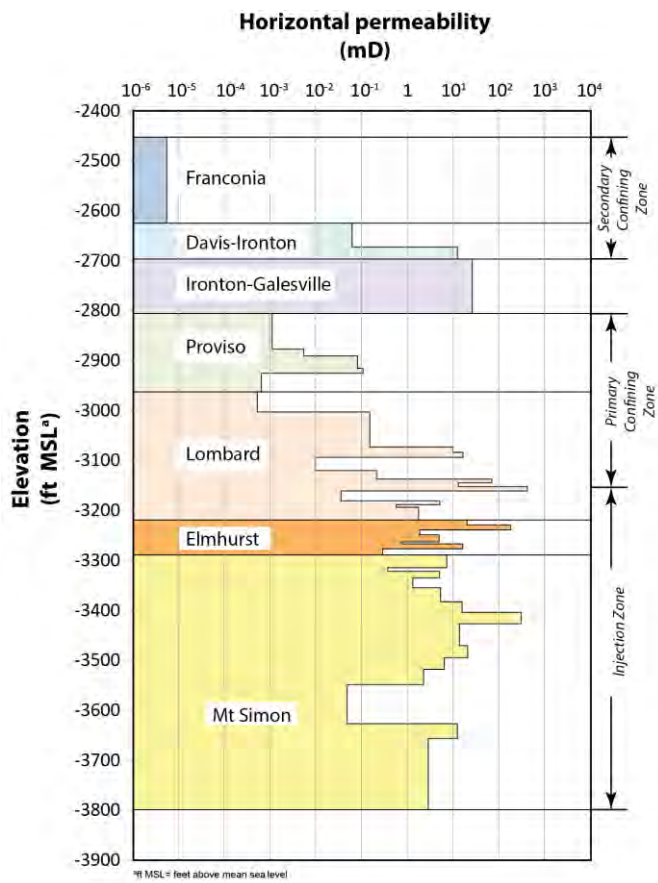

Figure 5. Vertical Distribution of the Horizontal Permeability in the Model Layers at the Stratigraphic Well Location

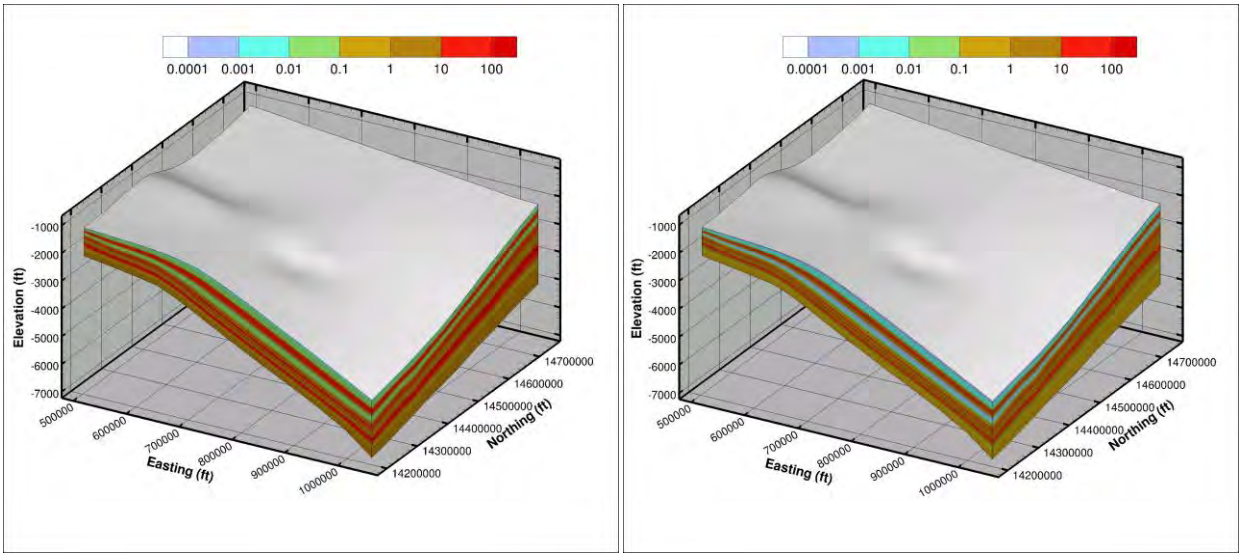

(a) **(b)**

Figure 6. Permeability Assigned to Numerical Model 1) Horizontal Permeability; b) Vertical Permeability

Table 1. Summary of the Hydrologic Properties Assigned to Each Model Layer. Depths and Elevations Correspond to the Location of the Stratigraphic Well

Simulation - CM22

	Model Layer	Top Depth (ft bgs)	Top Elevation (ft MSL)	Bottom Elevation (ft MSL)	Thickness (ft)	Porosity	Horizontal Permeability (mD)	Vertical Permeability (mD)	Grain Density (g/cm3)	Compresibility (1/Pa)
Secondary Conf. Zone	**Franconia**	3072.00	-2453	-2625	172	0.0358	5.50E-06	3.85E-08	2.82	7.42E-10
	Davis-Ironton3	3244.00	-2625	-2649	24	0.0367	6.26E-02	6.26E-03	2.73	3.71E-10
	Davis-Ironton2	3268.00	-2649	-2673	24	0.0367	6.26E-02	6.26E-03	2.73	3.71E-10
	Davis-Ironton1	3292.00	-2673	-2697	24	0.0218	1.25E+01	1.25E+00	2.73	3.71E-10
	Ironton-Galesville4	3316.00	-2697	-2725	28	0.0981	2.63E+01	1.05E+01	2.66	3.71E-10
	Ironton-Galesville3	3344.00	-2725	-2752	27	0.0981	2.63E+01	1.05E+01	2.66	3.71E-10
	Ironton-Galesville2	3371.00	-2752	-2779	27	0.0981	2.63E+01	1.05E+01	2.66	3.71E-10
	Ironton-Galesville1	3398.00	-2779	-2806	27	0.0981	2.63E+01	1.05E+01	2.66	3.71E-10
Primary Confining Zone	**Proviso5**	3425.00	-2806	-2877	71	0.0972	1.12E-03	1.12E-04	2.72	7.42E-10
	Proviso4	3496.00	-2877	-2891	14	0.0786	5.50E-03	5.50E-04	2.72	7.42E-10
	Proviso3	3510.00	-2891	-2916	25	0.0745	8.18E-02	5.73E-04	2.77	7.42E-10
	Proviso2	3534.50	-2916	-2926	10	0.0431	1.08E-01	7.56E-04	2.77	7.42E-10
	Proviso1	3544.50	-2926	-2963	38	0.0361	6.46E-04	4.52E-06	2.77	7.42E-10
	Lombard14	3582.00	-2963	-3003	40	0.1754	5.26E-04	5.26E-05	2.68	7.42E-10
	Lombard13	3622.00	-3003	-3038	35	0.0638	1.53E-01	1.53E-02	2.68	7.42E-10
	Lombard12	3657.00	-3038	-3073	35	0.0638	1.53E-01	1.53E-02	2.68	7.42E-10
	Lombard11	3692.00	-3073	-3084	11	0.0878	9.91E+00	9.91E-01	2.68	7.42E-10
	Lombard10	3703.00	-3084	-3094	10	0.0851	1.66E+01	1.66E+00	2.68	7.42E-10
	Lombard9	3713.00	-3094	-3121	27	0.0721	1.00E-02	1.00E-03	2.68	7.42E-10
	Lombard8	3739.50	-3121	-3138	17	0.0663	2.13E-01	2.13E-02	2.68	7.42E-10
	Lombard7	3756.50	-3138	-3145	8	0.0859	7.05E+01	7.05E+00	2.68	7.42E-10
	Lombard6	3764.00	-3145	-3153	8	0.0459	1.31E+01	1.31E+00	2.68	7.42E-10

Table 1. (contd)

	Model Layer	Top Depth (ft bgs)	Top Elevation (ft MSL)	Bottom Elevation (ft MSL)	Thickness (ft)	Porosity	Horizontal Permeability (mD)	Vertical Permeability (mD)	Grain Density (g/cm3)	Compresibility (1/Pa)
Injection Zone	**Lombard5**	3771.50	-3153	-3161	9	0.0760	4.24E+02	4.24E+01	2.68	7.42E-10
	Lombard4	3780.00	-3161	-3181	20	0.0604	3.56E-02	3.56E-03	2.68	7.42E-10
	Lombard3	3800.00	-3181	-3189	8	0.0799	5.19E+00	5.19E-01	2.68	7.42E-10
	Lombard2	3807.50	-3189	-3194	5	0.0631	5.71E-01	5.71E-02	2.68	7.42E-10
	Lombard1	3812.50	-3194	-3219	26	0.0900	1.77E+00	1.77E-01	2.68	7.42E-10
	Elmhurst7	3838.00	-3219	-3229	10	0.1595	2.04E+01	8.17E+00	2.64	3.71E-10
	Elmhurst6	3848.00	-3229	-3239	10	0.1981	1.84E+02	7.38E+01	2.64	3.71E-10
	Elmhurst5	3858.00	-3239	-3249	10	0.0822	1.87E+00	1.87E-01	2.64	3.71E-10
	Elmhurst4	3868.00	-3249	-3263	14	0.1105	4.97E+00	1.99E+00	2.64	3.71E-10
	Elmhurst3	3882.00	-3263	-3267	4	0.0768	7.52E-01	7.52E-02	2.64	3.71E-10
	Elmhurst2	3886.00	-3267	-3277	10	0.1291	1.63E+01	6.53E+00	2.64	3.71E-10
	Elmhurst1	3896.00	-3277	-3289	12	0.0830	2.90E-01	2.90E-02	2.64	3.71E-10
	MtSimon17	3908.00	-3289	-3315	26	0.1297	7.26E+00	2.91E+00	2.65	3.71E-10
	MtSimon16	3934.00	-3315	-3322	7	0.1084	3.78E-01	3.78E-02	2.65	3.71E-10
	MtSimon15	3941.00	-3322	-3335	13	0.1276	5.08E+00	2.03E+00	2.65	3.71E-10
	MtSimon14	3954.00	-3335	-3355	20	0.1082	1.33E+00	5.33E-01	2.65	3.71E-10
	MtSimon13	3974.00	-3355	-3383	28	0.1278	5.33E+00	2.13E+00	2.65	3.71E-10
	MtSimon12	4002.00	-3383	-3404	21	0.1473	1.59E+01	6.34E+00	2.65	3.71E-10
	MtSimon11	4023.00	-3404	-3427	23	0.2042	3.10E+02	1.55E+02	2.65	3.71E-10
	MtSimon10	4046.00	-3427	-3449	22	0.1434	1.39E+01	4.18E+00	2.65	3.71E-10
	MtSimon9	4068.00	-3449	-3471	22	0.1434	1.39E+01	4.18E+00	2.65	3.71E-10
	MtSimon8	4090.00	-3471	-3495	24	0.1503	2.10E+01	6.29E+00	2.65	3.71E-10
	MtSimon7	4114.00	-3495	-3518	23	0.1311	6.51E+00	1.95E+00	2.65	3.71E-10
	MtSimon6	4137.00	-3518	-3549	31	0.1052	2.26E+00	6.78E-01	2.65	3.71E-10
	MtSimon5	4168.00	-3549	-3588	39	0.1105	4.83E-02	4.83E-03	2.65	3.71E-10
	MtSimon4	4207.00	-3588	-3627	39	0.1105	4.83E-02	4.83E-03	2.65	3.71E-10
	MtSimon3	4246.00	-3627	-3657	30	0.1727	1.25E+01	1.25E+00	2.65	3.71E-10
	MtSimon2	4276.00	-3657	-3717	60	0.1157	2.87E+00	2.87E-01	2.65	3.71E-10
	MtSimon1	4336.00	-3717	-3799	82	0.1157	2.87E+00	2.87E-01	2.65	3.71E-10

Table 2. Lithology-Specific Permeability Anisotropy Averages from Literature

Facies or Lithology	Kv/Kh	Reference
1. Heterolithic, laminated shale/mudstone/siltstone/sandstone	0.1	Meyer and Krause (2006)
2. Herringbone cross-stratified sandstone. Strat dips to 18 degrees	0.4	Meyer and Krause (2006)
3. Paleo weathered sandstone (coastal flat)	0.4	Meyer and Krause (2006)
4. Accretionary channel bar sandstones with minor shale laminations	0.5	Ringrose et al. (2005); Meyer and Krause (2006)
6. Alluvial fan, alluvial braided stream plain to shallow marine sandstones, low clay content	0.3	Kerr et al. (1999)
7. Alluvial fan, alluvial plain sandstones, sheet floods, paleosols, higher clay content	0.1	Hornung and Aigner (1999)
8. Dolomite mudstone	0.007	Saller et al. (2004)

Table 3. Summary of the K_v/K_h Ratios Applied to Model Layers

Model Layer	Kv/Kh Applied to Model Layers[(a)]*	Kv/Kh Determined from Core Pairs[(b)]	Successfully Analyzed Core Pairs
Franconia carbonate	0.007	ND	ND
Davis-Ironton	0.1	ND	ND
Ironton-Galesville	0.4	ND	ND
Proviso (Layers 4 and 5)	0.1	ND	ND
Proviso ([carbonate] Layers 1 to 3)	0.007	ND	ND
Lombard Total Interval	0.1	0.029	12
Lombard (Layer 7)	0.1	.098	2
Lombard (Layer 6)	0.1	0.003	2
Lombard (Layer 5)	0.1	ND	ND
Lombard (Layer 4)	0.1	0.016	2
Lombard (Layer 3)	0.1	0.064	2
Lombard (Layer 2)	0.1	0.009	1
Lombard (Layer 1)	0.1	0.104	3
Elmhurst Total Interval	0.4	0.06	4
Elmhurst (Layer 7)	0.4	ND	ND
Elmhurst (Layer 6)	0.4	0.023	1
Elmhurst (Layer 5)	0.1	ND	ND
Elmhurst (Layer 4)	0.4	0.902	1
Elmhurst (Layer 3)	0.1	ND	ND
Elmhurst (Layer 2)	0.4	0.022	1
Elmhurst (Layer 1)	0.1	0.037	1
Mt. Simon (Layer 17)	0.4	0.233	2
Mt. Simon (Layer 16)	0.1	ND	ND
Mt. Simon (layer 13)	0.4	0.643	2
Mt. Simon (Layers 12, 14, and 15)	0.4	ND	ND
Mt. Simon (Layer 11, Injection) zone)	0.5	ND	ND
Mt. Simon (Layers 6, 7, 8, 9, 10)	0.3	ND	ND
Mt. Simon (Layers 1, 2, 3, 4, 5)	0.1	ND	ND

(a) Value from literature, referenced in the Supporting Documentation of the UIC permit application
(b) Geometric mean of successful core pairs.

Porosity

Total (or absolute) porosity is the ratio of void space to the volume of whole rock. Effective porosity is the ratio of interconnected void space to the volume of the whole rock. As a first step in assigning porosity values for the FutureGen 2.0 numerical model layers, Schlumberger ELAN porosity log results were compared with laboratory measurements of porosity as determined from SWC and core plugs for specific sampling depth within the Mount Simon. The Schlumberger ELAN porosity logs examined include PIGN (Gamma-Neutron Porosity), PHIT (Total Porosity), and PIGE (Effective Porosity). The PIGN and PIGE wireline log surveys use different algorithms to identify clay- or mineral-bound fluid/porosity in calculating an effective porosity value. SWC porosity measurements are listed as "total porosity," but their measurement can be considered to be determinations of "effective porosity," because the measurement technique (weight measurements of heated/oven-dried core samples) primarily measures the amount of "free" or connected pore liquid contained within the SWC sample as produced by the heating process. It should be noted that the SWC porosity measurements were determined under ambient pressure conditions.

In Figure 2, neutron- and density-crossplot porosity is shown in the fourth panel, along with lab-measured porosity for core plugs and rotary SWC. An available porosity measurement data set for a conventional Mount Simon Sandstone core-plug sample taken near the top of the formation (depth of 3,912 ft bgs or elevation of -3,293 ft) indicates only minor changes in porosity for measurements taken over a wide range in pressure (i.e., ambient to 1,730 psi). This suggests that ambient SWC porosity measurements of the Mount Simon may be representative of in situ formation pore pressure conditions. The ELAN porosity log results generally underestimate the SWC porosity measured values. As a result of the poor visual correlation of the PIGE survey results with SWC measurements, this ELAN log was omitted from subsequent correlation evaluations. To aid in the correlations, the gamma ray survey log (GR) was used as a screening tool for development of linear-regression correlation relationships between ELAN log responses and SWC porosity measurements. This helps account for the shale or clay content that can cause the inclusion of "bound water" porosity. To assign model layer porosities, the regression model relationships used to calibrate the ELAN measurement results (Figure 7) were applied to the ELAN survey results over the formational depths represented by the Mount Simon (3,904 to 4,416 ft bgs depth or -3,285 to -3,797 ft elevation) and overlying Eau Claire-Elmhurst member (3,838 to 3,904 ft bgs depth or -3,219 to -3,285 ft elevation) based on the gamma response criteria. The ELAN survey results are reported at 0.5-ft depth intervals. For stratigraphic units above the Elmhurst and/or depth intervals exhibiting gamma readings >64 API units, the un-calibrated, average ELAN log result for that depth interval was used. An average porosity was then assigned to the model layer based on the average of the calibrated ELAN values within the model layer depth range. Figure 8 shows the depth profile of the assigned model layer porosities based on the average of the calibrated ELAN values. The actual values assigned for each layer are listed in Table 1.

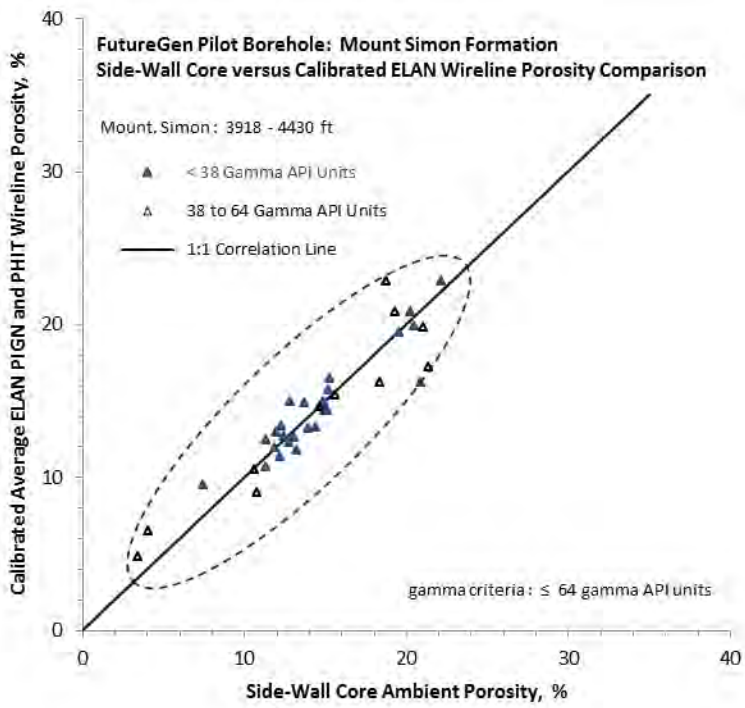

Figure 7. Comparison of SWC Porosity Measurements and Regression-Calibrated ELAN Log Porosities: ≤64 Gamma API Units

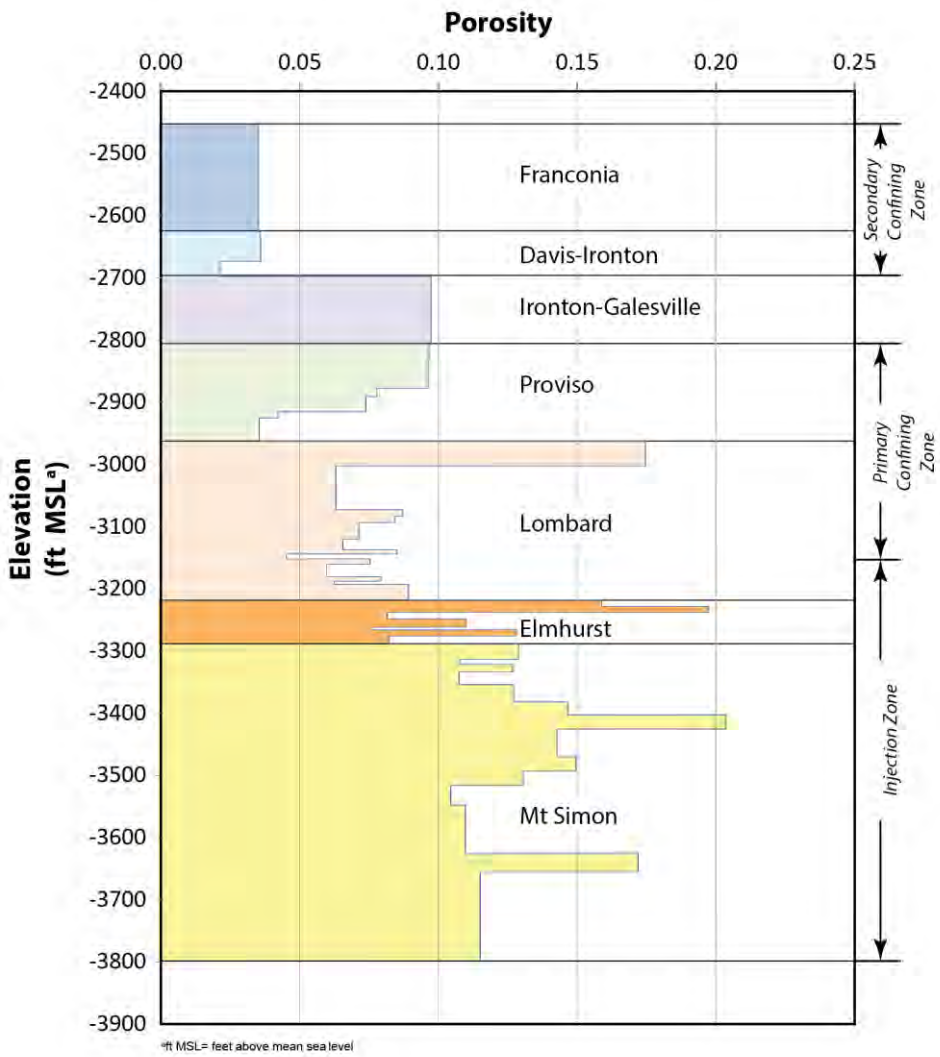

Figure 8. Vertical Distribution of Porosity in the Model Layers at the Stratigraphic Well Location

Rock (Bulk) Density and Grain Density

Grain density data were calculated from laboratory measurements of SWCs. The data were then averaged (arithmetic mean) for each main stratigraphic layer in the model. Only the Proviso member (Eau Claire Formation) has been divided in two sublayers to be consistent with the lithology changes. Figure 9 shows the calculated grain density with depth. The actual values assigned to each layer of the model are listed in Table 1. Grain density is the input parameter specified in the simulation input file, and STOMP-CO2 calculates the bulk density from the grain density and porosity for each model layer.

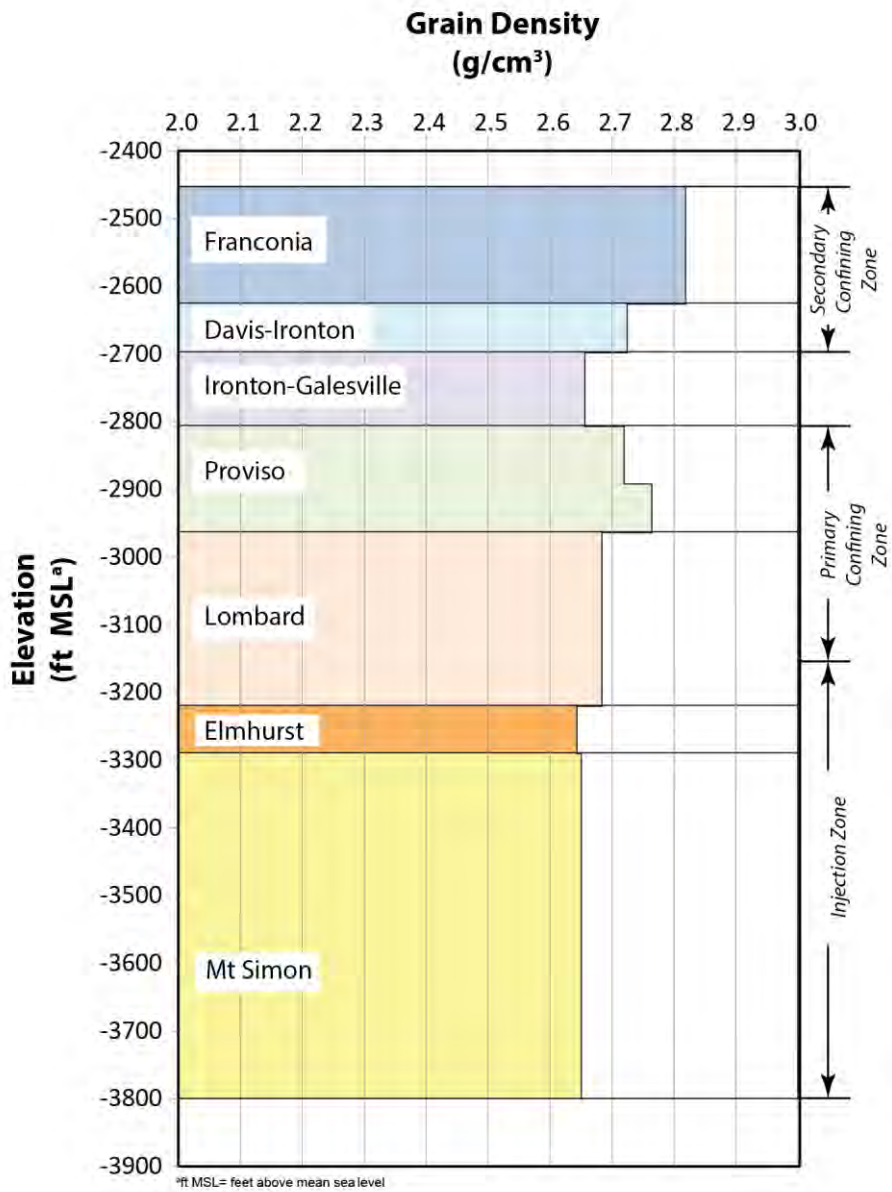

Figure 9. Vertical Distribution of the Grain Density in the Model Layer at the Stratigraphic Well Location

Formation Compressibility

Limited information about formation (pore) compressibility estimates is available. The best estimate for the Mount Simon Sandstone (Table 4) is that back-calculated by Birkholzer et al. (2008) from a pumping test at the Hudson Field natural-gas storage site, found 80 mi (129 km) northeast of the Morgan County CO_2 storage site. The back-calculated pore-compressibility estimate for the Mount Simon Sandstone of 3.71E−10 Pa^{-1} was used as a spatially constant value for their basin-scale simulations. In other simulations, Birkholzer et al. (2008) assumed a pore-compressibility value of 4.5E−10 Pa^{-1} for aquifers and 9.0E−10 Pa^{-1} for aquitards. Zhou et al. (2010) in a later publication used a pore-compressibility value of 7.42E−10 Pa^{-1} for both the Eau Claire Formation and Precambrian granite, which were also used for these initial simulations

(Table 4). Because the site-specific data are limited to a single reservoir sample, only these two published values have been used for the model. The first value (3.71E-10 Pa^{-1}) has been used for sands that are compressible because of the presence of porosity. The second value (7.42E-10 Pa^{-1}) is assigned for all other rocks that are less compressible (dolomite, limestone, shale, and rhyolite). Table 1 lists the hydrologic parameters assigned to each model layer.

Table 4. Formation Compressibility Values Selected from Available Sources

Hydrogeologic Unit	Formation (Pore) Compressibility, Pa^{-1}
Franconia	7.42E-10 Pa-^{1}
Davis-Ironton	3.71E-10 Pa^{-1}
Ironton-Galesville	3.71E-10 Pa^{-1}
Eau Claire Formation (Lombard and Proviso)	7.42E-10 Pa^{-1}
Eau Claire Formation (Elmhurst)	3.71E-10 Pa^{-1}
Mount Simon Sandstone	3.71E-10 Pa^{-1}

Constitutive Relationships

Capillary Pressure and Saturation Functions

Capillary pressure is the pressure difference across the interface of two immiscible fluids (e.g., CO_2 and water). The entry capillary pressure is the minimum pressure required for an immiscible non-wetting fluid (i.e., CO_2) to overcome the capillary force and enter pore space containing the wetting fluid (i.e., saline formation water). Capillary pressure data determined from site-specific cores were not available at the time the model was constructed. However, tabulated capillary pressure data were available for several Mount Simon gas storage fields in the Illinois Basin. The data for the Manlove Hazen well (FutureGen Alliance 2006) were the most complete. Therefore, these aqueous saturation and capillary pressure values were plotted and a user-defined curve fitting was performed to generate Brooks-Corey parameters for four different permeabilities (Figure 10). These parameters were then assigned to layers based on a permeability range as shown in Table 5.

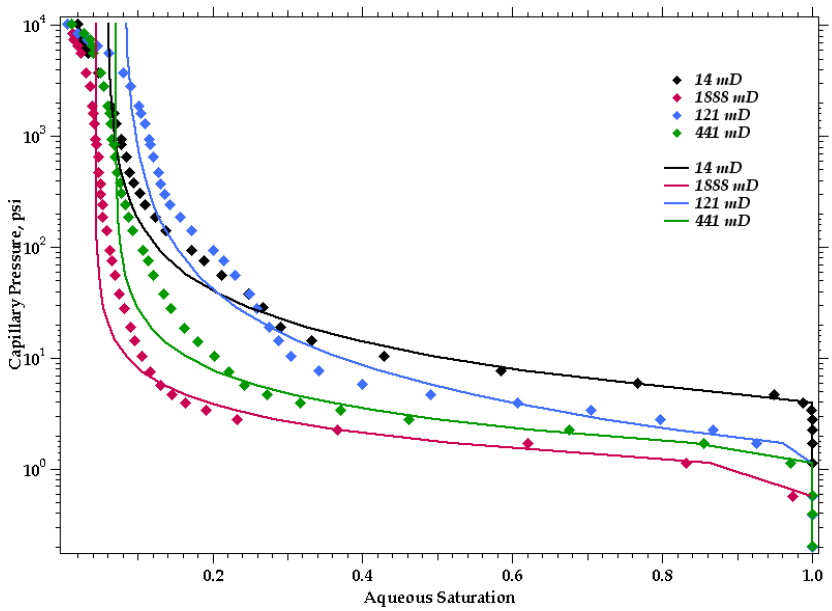

Figure 10. Aqueous Saturation Versus Capillary Pressure Based on Mercury Injection Data from the Hazen No. 5 Well at the Manlove Gas Field in Champagne County, Illinois

Table 5. Permeability Ranges Used to Assign Brooks-Corey Parameters to Model Layers

Permeability (mD)	Psi	Lambda (λ)	Residual Aqueous Saturation
< 41.16	4.116	0.83113	0.059705
41.16 to 231	1.573	0.62146	0.081005
231 to 912.47	1.450	1.1663	0.070762
> 912.47	1.008	1.3532	0.044002

The Brooks-Corey (1964) saturation function is given as

$$S_{ew} = \begin{cases} (P_e / P_c)^{\lambda} & if \quad P_c > P_e \\ 1 & otherwise \end{cases}$$

where S_{ew} is effective aqueous saturation, P_c is capillary pressure, P_e is gas entry pressure, and λ is the pore-size distribution parameter. Combined with the Burdine (1953) relative permeability model, the relative permeability for the aqueous phase, k_{rw}, and that for the non-aqueous phase, k_{rn}, are

$$K_{rw} = (S_{ew})^{3+2/\lambda}$$

$$K_{rn} = (1 - S_{ew})^2 (1 - S_{ew}{}^{1+2/\lambda})$$

Values for the residual aqueous saturation (S_{rw}) and the two other parameters used in the Brooks-Corey capillary pressure-saturation function (i.e., the non-wetting fluid entry pressure and a pore-size distribution parameter) were all obtained by fitting mercury (Hg) intrusion-capillary pressure data from the Manlove gas storage site in Champaign County. The fitting was applied after scaling the capillary pressures to account for the differences in interfacial tensions and contact angles for the brine-CO_2 fluid pair, relative to vapor-liquid Hg used in the measurements.

This approach has the major advantage that the three fitted parameters are consistent as they are obtained from the same original data set. The use of consistent parameter values is not the norm for brine-CO_2 flow simulations in the Mount Simon Sandstone.

The S_{rw} values used in the modeling (Table 2) are indeed lower than the values found in the literature. The FutureGen Alliance was aware of these differences but opted to use a consistent data set for all retention parameter values instead of selecting parameter values from different data sources. An additional reason for using this approach is the considerable uncertainty in S_{rw} values for Mt. Simon rock in the literature. In general, using a lower S_{rw} value for the injection zone will possibly result in a somewhat smaller predicted CO_2 plume size and a smaller spatial extent of the pressure front compared to using a higher value of S_{rw}. Variation of S_{rw} in the confining zone (cap rock) likely has relatively little impact on CO_2 transport and pressure development owing to the typically much lower permeability of this zone relative to the underlying formation.

Gas Entry Pressure

No site-specific data were available for gas entry pressure; therefore, this parameter was estimated using the Davies (1991) developed empirical relationships between air entry pressure, *Pe*, and intrinsic permeability, *k*, for different types of rock:

$$Pe = a\,k^b$$

where *Pe* takes the units of MPa and *k* the units of m^2, *a* and *b* are constants and are summarized below for shale, sandstone, and carbonate (Davies 1991; Table 3). The dolomite found at the Morgan County site is categorized as a carbonate. The *Pe* for the air-water system is further converted to that for the CO_2-brine system by multiplying the interfacial tension ratio of a CO_2-brine system β_{cb} to an air-water system β_{aw}. An approximate value of 30 mN/m was used for β_{cb} and 72 mN/m for β_{aw}.

Table 6. Values for Constants a and b for Different Lithologies

	Shale	Sandstone	Carbonate
a	7.60E-07	2.50E-07	8.70E-07
b	-0.344	-0.369	-0.336

CO_2 Entrapment

The entrapment option available in STOMP-CO2 was used to allow for entrapment of CO_2 when the aqueous phase is on an imbibition path (i.e., increasing aqueous saturation). Gas saturation can be free or trapped:

$$s_g = 1 - s_l = s_{gf} + s_{gt}$$

where the trapped gas is assumed to be in the form of aqueous occluded ganglia and immobile. The potential effective trapped gas saturation varies between zero and the effective maximum trapped gas saturation as a function of the historical minimum value of the apparent aqueous saturation. No site-specific data were available for the maximum trapped gas saturation, so this value was taken from the literature. Suekane et al. (2009) used micro-focused x-ray CT to image

a chip of Berea Sandstone to measure the distribution of trapped gas bubbles after injection of $scCO_2$ and then water, under reservoir conditions. Based on results presented in the literature, a value of 0.2 was used in the model, representing the low end of measured values for the maximum trapped gas saturation in core samples.

Formation Properties

Fluid Pressure

An initial fluid sampling event from the Mount Simon formation was conducted on December 14, 2011, in the stratigraphic well during the course of conducting open-hole logging. Sampling was attempted at 22 discrete depths using the MDT tool in the Quicksilver Probe configuration and from one location using the conventional (dual-packer) configuration. Pressure data were obtained at 7 of the 23 attempted sampling points, including one duplicated measurement at a depth of 4,034 ft bgs or elevation of -3415 ft (Table 7).

Figure 11 shows the available regional potentiometric surfaces for the Mount Simon Sandstone. The figure contains pre-development hydraulic head measurements (e.g., before widespread pumping from the Mount Simon Sandstone, particularly in Northern Illinois) and simulation results for predicting the post-development (i.e., 1980) potentiometric surface. As shown in Figure 11, data are sparse around the area of the FutureGen 2.0 Site, and it is situated in an area where the regional gradients are very low and the flow directions are not constrained (pre- or post-development). For these reasons, a regional horizontal flux for the Mount Simon Sandstone was not specified in the computational model.

Vertical flow potential at the FutureGen 2.0 Site was evaluated based on an analysis of discrete pressure/depth measurements obtained within the pilot characterization borehole over the depth interval of 1,134 to 4,249 ft bgs depth (-515 to -3,630 ft elevation). The results indicate that there is a positive head difference in the Mount Simon that ranges from 47.8 to 61.6 ft above the calculated St. Peter observed static hydraulic head condition (i.e., 491.1 ft above MSL). This positive head difference suggests a natural vertical flow potential from the Mount Simon to the overlying St. Peter if hydraulic communication is afforded (e.g., an open communicative well). It should also be noted, however, that the higher head within the unconsolidated Quaternary aquifer (~611 ft above MSL), indicates a downward vertical flow potential from this surficial aquifer to both the underlying St. Peter and Mount Simon bedrock aquifers. The disparity in the calculated hydraulic head measurements (together with the significant differences in formation fluid salinity) also suggests that groundwater within the St. Peter and Mount Simon bedrock aquifers is physically isolated from one another. This is an indication that there are no significant conduits (open well bores or fracturing) between these two formations and that the Eau Claire forms an effective confining layer.

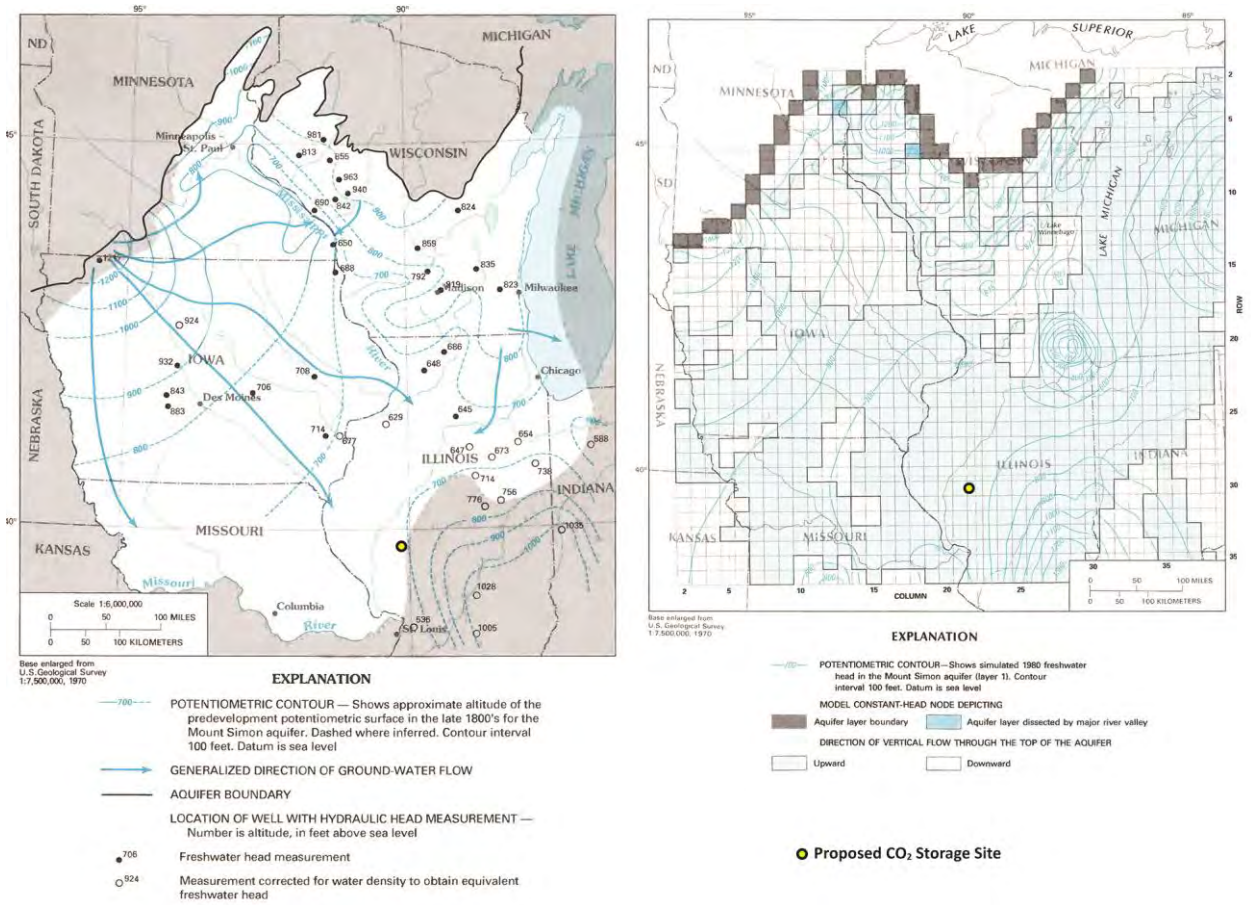

Figure 11. Approximate Pre-Development Potentiometric Surface (a) for the Mount Simon Aquifer (from Young 1992, modified from Mandel and Kontis 1992) and (b) Simulated 1980 Freshwater Head in the Mount Simon Aquifer showing Impact of Withdrawals in Northern portion of Illinois (Mandel and Kontis 1992)

Table 7. Pressure Data Obtained from the Mount Simon Formation Using the MDT Tool Where the Red Line Delimits the Samples Within the Injection Zone

Sample Number	Sample Depth (ft bgs)	Absolute Pressure (psia)
7	4,116	1,828
8	4,117	1,827.7
9	4,096.5	1,818.3
11	**4,034**	**1,790.2**
17	**4,034 (duplicated)**	**1,790.3**
21	4,234.5	1,889.2
22	4,232	1,908.8
23	4,249	1,896.5[(a)]

(a) Sample affected by drilling fluids (not representative)

Temperature

The best fluid temperature depth profile was performed on February 9, 2012, as part of the static borehole flow meter/fluid temperature survey that was conducted prior to the constant-rate injection flow meter surveys. Two confirmatory discrete probe depth measurements that were taken prior to the active injection phase (using colder brine) corroborate the survey results. The discrete static measurement for the depth of 3,698 ft bgs (elevation of -3,079 ft) was 95.9°F. The second discrete static probe temperature measurement is from the MDT probe for the successful sampling interval of 4,034 ft bgs depth (elevation of -3,415 ft). A linear-regression temperature/depth relationship was developed for use by modeling. The regression data set analyzed was for temperature data over the depth interval of 1,286 to 4,533 ft bgs (elevation of -667 to -3,914 ft). Based on this regression, a projected temperature for the reference datum at the top of the Mount Simon (3,904 ft bgs depth or -3,285 ft elevation) of 96.60°F is indicated. A slope (gradient) of 6.72×10^{-3} °F/ft and intercept of 70.27°F is also calculated from the regression analysis.

Brine Density

Although this parameter is determined by the simulator using pressure, temperature, and salinity, based on the upper and lower Mount Simon injection zone tests, the calculated in situ injection zone fluid density is 1.0315 g/cm^3.

Salinity and Water Quality

During the process of drilling the well, fluid samples were obtained from discrete-depth intervals in the St. Peter Formation and the Mount Simon Formation using wireline-deployed sampling tools (MDTs) on December 14, 2011. After the well had been drilled, additional fluid samples were obtained from the open borehole section of the Mount Simon Formation by extensive pumping using a submersible pump. The assigned salinity value for the Mount Simon (upper zone) 47,500 ppm is as indicated by both the MDT sample (depth 4,034 ft bgs or elevation of -

3,415 ft) and the multiple samples collected during extensive composite pumping of the open borehole section.

A total of 20 groundwater samples were collected between October 25 and November 10, 2011, including duplicate samples and blanks (Dey et al. in press as of 2013). General water-quality parameters were measured along with organic and major inorganic constituents. Values of pH ranged from 7.08 to 7.66. Values for specific conductance ranged from 545 to 1,164 µS/cm, with an average of 773 µS/cm. Values of Eh ranged from 105 to 532 mV with an average of 411 mV. Values of dissolved oxygen (DO) ranged from below detection limit to 3.3 mg/L O_2. Most dissolved inorganic constituent concentrations are within primary and secondary drinking water standards. However, the constituent concentration in water is elevated with respect to iron (Fe), manganese (Mn), nitrate (NO3), and the total dissolved salt (TDS). In some cases these constituents exceed the U.S. Environmental Protection Agency (EPA) secondary standards.

Fracture Pressure in the Injection Zone

At the time the computational model was developed, no site-specific hydraulic fracturing tests had been conducted in the stratigraphic well and no site-specific fracture pressure values were available for the confining zone and the injection zone. Other approaches (listed below) have thus been chosen to determine an appropriate value for the fracture pressure.

- Triaxial tests were conducted on eight samples from the stratigraphic well. Samples 3 to 7 are located within the injection zone. Fracture gradients were estimated to range from 0.647 to 0.682 psi/ft, which cannot directly be compared to the fracture pressure gradient required for the permit. Triaxial tests alone cannot provide accurate measurement of fracture pressure.
- Existing regional values. Similar carbon storage projects elsewhere in Illinois (in Macon and Christian counties) provide data for fracture pressure in a comparable geological context. In Macon County (CCS#1 well at Decatur), about 65 mi east of the FutureGen 2.0 Site, a fracture pressure gradient of 0.715 psi/ft was obtained at the base of the Mount Simon Sandstone Formation using a step-rate injection test (EPA 2011a). In Christian County, a "conservative" pressure gradient of 0.65 psi/ft was used for the same injection zone (EPA 2011b). No site-specific data were available.
- Last, the regulation relating to the "Determination of Maximum Injection Pressure for Class I Wells" in EPA Region 5 is based on the fracture closure pressure, which has been chosen to be 0.57 psi/ft for the Mount Simon Sandstone (EPA 1994).

Based on these considerations, a fracture pressure gradient of 0.65 psi/ft was chosen. The EPA Geologic Sequestration Rule requires that "Except during stimulation, the owner or operator must ensure that injection pressure does not exceed 90 percent of the fracture pressure of the injection zone(s) so as to ensure that the injection does not initiate new fractures or propagate existing fractures in the injection zone(s)…" Therefore, a value of 0.585 psi/ft (90 percent of 0.65 psi/ft) was used in the model to calculate the maximum injection pressure permitted.

In November and December 2013, hydraulic tests were conducted in the Mount Simon Sandstone and in the Precambrian basement. The first results of these tests verify that the fracture gradient used in the model for the injection zone remains conservative and appropriate.

Site Evaluation of Mineral Resources

Other subsurface geochemical considerations include the potential for mineral or hydrocarbon resources beneath the proposed CO_2 storage site. While no significant mineral deposits are known to exist within Morgan County, natural gas has been recovered in the region, including at the Prentice and Jacksonville fields located within several miles of the stratigraphic well. ISGS oil and gas website data indicate that the Prentice Field contained more than 25 wells drilled during the 1950s; re-exploration occurred in the 1980s. Both oil and gas have been produced from small stratigraphic traps in the shallow Pennsylvanian targets, at depths of 250 to 350 ft (75 to 105 m) bgs. It is important to note that gas produced from these wells may contain around 16 percent CO_2 (Meents 1981). More than 75 wells have been drilled in the Jacksonville Field. Gas was discovered in the Jacksonville Field as early as 1890 (Bell 1927), but most oil and gas production from the Prentice and Jacksonville fields occurred between the late 1920s and late 1980s. The most productive formations in the Illinois Basin (lower Pennsylvanian and Mississippian siliciclastics and Silurian reefs) are not present in Morgan County. Only two boreholes in the vicinity of the Prentice Field and five boreholes near the Jacksonville Field penetrate through the New Albany Shale into Devonian and Silurian limestone. Cumulative production from the Prentice and Jacksonville fields is not available, and both fields are largely abandoned. The Waverly Storage Field natural-gas storage site in the southeast corner of Morgan County originally produced oil from Silurian carbonates. This field no longer actively produces oil, but since 1954 it has been successfully used for natural-gas storage in the St. Peter and the Galesville/Ironton Sandstone formations (Buschbach and Bond 1974).

The nearest active coal mine is approximately 10 mi (16 km) away in Menard County and does not penetrate more than 200 ft (61 m) bgs (ISGS 2012). A review of the known coal geology within a 5-mi (8-km) radius of the proposed drilling site indicates that the Pennsylvanian coals, the Herrin, Springfield, and Colchester coals, are very thin or are absent from the project area (ISGS 2010, 2011; Hatch and Affolter 2008). During continuous coring of a shallow groundwater monitoring well located immediately adjacent to the stratigraphic well, only a single thin (5-ft [1.5-m]) coal seam was encountered at about 200 ft (61 m) depth.

Initial Conditions

The injection zone is assumed to be under hydrostatic conditions with no regional or local flow conditions. Therefore the hydrologic flow system is assumed to be at steady state until the start of injection. To achieve this with the STOMP-CO2 simulator one can either run an initial simulation (executed for a very long time period until steady-state conditions are achieved) to generate the initial distribution of pressure, temperature, and salinity conditions in the model from an initial guess, or one can specify the initial conditions at a reference depth using the hydrostatic option in the STOMP-CO2 input file, allowing the simulator to calculate and assign the initial conditions to all the model nodes. Site-specific data were available for pressure, temperature, and salinity, and therefore the hydrostatic option was used to assign initial conditions. A temperature gradient was specified based on the geothermal gradient, but the initial

salinity was considered to be constant for the entire domain. A summary of the initial conditions is presented in Table 8.

Table 8. Summary of Initial Conditions

Parameter	Reference Depth (ft bgs)	Elevation (ft)	Value
Reservoir Pressure	4,034	-3,415	1,790.2 psi
Aqueous Saturation			1.0
Reservoir Temperature	3,904	-3,285	96.6 °F
Temperature Gradient			0.00672 °F/ft
Salinity			47,500 ppm

Boundary Conditions

Boundary conditions were established with the assumption that the injection zone and confining zone are continuous throughout the region and that the underlying Precambrian unit is impermeable. Therefore, the bottom boundary was set as a no-flow boundary for aqueous fluids and for the CO_2-rich phase. The lateral and top boundary conditions were set to hydrostatic pressure using the initial condition with the assumption that each of these boundaries is distant enough from the injection zone to have minimal to no effect on the CO_2 plume migration and pressure distribution.

Wells within the Survey Area

A detailed survey was completed over a 25 mi^2 (65 km^2) area, termed the "Survey Area." This area is centered on the proposed injection location (labeled as "Injection Site") and encompasses the predicted maximum extent of the CO_2 plume (Figure 12). Wells, surface bodies of water and other pertinent surface features, administrative boundaries, and roads within the Survey Area are shown in Figure 12. There are no subsurface cleanup sites, mines, quarries, or Tribal lands within this area. The Survey Area is near the center of the AoR (Figure 15).

A total of 129 wells are located within the Survey Area. However, no well but the FutureGen Alliance's stratigraphic well penetrates the injection zone (Mount Simon Sandstone and the lower Eau Claire [Elmhurst Sandstone Member and lower portion of the Lombard Member]), the confining zone (Upper portion of Lombard Member and Proviso Member of the Eau Claire Formation), or the secondary confining zone (Franconia Dolomite).

Shallow domestic water wells with depths of less than 50 ft (15 m) are the most common well type within the Survey Area. Five slightly deeper water wells were identified that range in depths from 110 ft (33 m) to 405 ft (123 m). Other wells include stratigraphic test holes, coal test holes, and oil and gas wells.

Twenty four of the 129 wells in the Survey Area are identified with only a general location (center of a section) in the ISWS database. These wells are included in Table 9 but are not shown on the map.

A general survey of the AoR outside the Survey Area was conducted by reference of publicly available information. Maps of existing water wells, oil and gas wells, miscellaneous wells, coal mines, surface water, and geologic structures were submitted to complete the permit requirements.

There are 4,386 water wells and 740 oil and gas wells within the AoR, but only two of these penetrate the confining zone. These two wells identified in the AoR are approximately 16 miles from the injection site, but they are adequately plugged.

Table 9. List of Wells Located Within the Survey Area

Map ID	API Number	ISWS ID	Latitude NAD1983	Longitude NAD1983	Public Land Survey System	Total Depth ft	Elev ft	Completion Date	Owner	Well Num	Well Type	Status	Confining Zone Penetration Well
0	121372213200		39.806064	-90.052919	T16n,R9w,Sec 25	4812	633	TBD	FutureGen Industrial Alliance, Inc.	1	Monitoring	Active	Yes
1	121372118200	116519	39.778074	-90.078443	T15N,R9W,Sec 2	25		19780712	A.A. Negus Estate	1	Water	Private Water Well	No
4	121370018700	115778	39.811025	-90.065241	T16N,R9W,Sec 25	115			Beilschmidt, William H.		Water		No
8	121370028500	115740	39.800661	-90.078386	T16N,R9W,Sec 26	127		1950	Martin, L. E.	1	Water		No
9		115741	39.800661	-90.078386	T16N,R9W,Sec 26	127			Martin, L. E.		Water		No
10	121372128600	115779	39.801129	-90.07342	T16N,R9W,Sec 26	25		19781213	Martin, Marvin & Jean	1	Water	Private Water Well	No
14		115763	39.792894	-90.078875	T16N,R9W,Sec 35	28			E Clemons		Water		No
15		115764	39.792894	-90.078875	T16N,R9W,Sec 35	25			B Sister		Water		No
16		115765	39.792837	-90.060294	T16N,R9W,Sec 36	35			J M Dunlap		Water		No
17	121370051100		39.792893	-90.078984	T16N,R9W,Sec 35	1056	643		O'Rear, Judge	1	Oil & Gas / Water		No
18	121370009900		39.808545	-90.06614	T16N,R9W,Sec 25	1530	630	19391001	Beilschmidt, Wm.	1	Oil & Gas	Dry and Abandoned, No Shows	No
19	121370023500		39.779153	-90.077325	T15N,R9W,Sec 2	338	644	19231101	Conklin	1	Oil & Gas	Dry and Abandoned, No Shows	No
20	121370023600		39.781298	-90.075082	T15N,R9W,Sec 2	348	646	19231101	Conklin	2	Oil & Gas	Dry and Abandoned, No Shows	No
21	121370023700		39.778057	-90.080754	T15N,R9W,Sec 3	342	645	19231001	Harris, A. J.	1	Oil & Gas	Gas Producer	No
22	121370023900		39.7779	-90.080756	T15N,R9W,Sec 3	334	644	19231107	Harris, A. J.	3	Oil & Gas	Gas Producer	No
25	121370036300		39.805251	-90.075597	T16N,R9W,Sec 26	1205		19670330	Martin	1	Oil & Gas	Dry and Abandoned, No Shows	No
26	121370036301		39.805251	-90.075597	T16N,R9W,Sec 26	1400		19731029	Martin	1	Oil & Gas	Junked and Abandoned, Plugged	No
27	121372088500		39.800861	-90.073017	T16N,R9W,Sec 26	302	630				Coal Test		No
		115735	39.807386	-90.060378	T16N,R9W,Sec 25	27			Beilschmidt, William H.		Water		No
		115736	39.807386	-90.060378	T16N,R9W,Sec 25	30			W R Fowler		Water		No
		115737	39.807386	-90.060378	T16N,R9W,Sec 25	28			Mason		Water		No
		115739	39.807478	-90.079049	T16N,R9W,Sec 26	25			C H Matin		Water		No
		115738	39.807478	-90.079049	T16N,R9W,Sec 26	22			T Gondall		Water		No
		115650	39.807193	-90.041413	T16N,R8W,Sec 30	19		1930	R Allison		Water		No
		115651	39.792765	-90.041512	T16N,R8W,Sec 31	28			W J Huston		Water		No
		115652	39.792765	-90.041512	T16N,R8W,Sec 31	28			E Robinson		Water		No
		116450	39.777005	-90.052023	T15N,R9W,Sec 1	25			A Harris		Water		No
		116453	39.776968	-90.070521	T15N,R9W,Sec 2	32			A Harris		Water		No
		116451	39.776968	-90.070521	T15N,R9W,Sec 2	22			W R Conklin		Water		No
		116452	39.776968	-90.070521	T15N,R9W,Sec 2	30			B Negus		Water		No
		116454	39.77688	-90.088996	T15N,R9W,Sec 3	28			C Negus		Water		No
		116455	39.77688	-90.088996	T15N,R9W,Sec 3	30			L B Trotter		Water		No
		115727	39.821881	-90.078925	T16N,R9W,Sec 23	30			D Flinn		Water		No
		115728	39.821881	-90.078925	T16N,R9W,Sec 23	30			Hazel Dell School		Water		No
		115729	39.821881	-90.078925	T16N,R9W,Sec 23	35			K Haneline		Water		No
		115733	39.821811	-90.060168	T16N,R9W,Sec 24	30			J L Icenagle		Water		No
		115734	39.821811	-90.060168	T16N,R9W,Sec 24	30			G Lewis		Water		No
		115775	39.821811	-90.060168	T16N,R9W,Sec 24	200		1944	E C Lewis		Water		No
		115742	39.807531	-90.097566	T16N,R9W,Sec 27	23			J Stewart		Water		No
		115743	39.807531	-90.097566	T16N,R9W,Sec 27	23			l J Stewart		Water		No
		115761	39.792917	-90.097513	T16N,R9W,Sec 34	28			T Harrison		Water		No
		115762	39.792917	-90.097513	T16N,R9W,Sec 34	30			J Mahon		Water		No

Map ID	API Number	ISWS ID	Latitude (NAD 83)	Longitude (NAD 83)	Public Land Survey System (PLSS)	Total Depth (ft)	Elevation (ft)	Completion Date	Owner	Well #	Well Type	Status	Confining Zone Penetration Well
2	121372155200	237387	39.815638	-90.084967	T16N,R9W,Sec 23	41		19920313	Nickel, Gerald	1	Water	Private Water Well	No
3	121372182100	300966	39.815638	-90.084967	T16N,R9W,Sec 23	46		19971104	Nickel, Gerald & Diane	1	Water	Private Water Well	No
13	121372173400	297871	39.811987	-90.07805	T16N,R9W,Sec 26	37		19960213	Keltner, Dale		Water	Private Water Well	No
23	121370024000		39.780186	-90.094859	T15N,R9W,Sec 3	402	642	19230101	Trotter, L.B.	1	Oil & Gas	Dry and Abandoned, No Shows	No
24	121372097800		39.776078	-90.080727	T15N,R9W,Sec 3	327	632	0	Harris		Unknown / other	Unknown, Plugged	No
28		115642	39.82166	-90.041238	T16N,R8W,Sec 19	25		1870	W W Robertson		Water		No
38		116456	39.776761	-90.107843	T15N,R9W,Sec 4	30			Rayburn		Water		No
39		116457	39.776761	-90.107843	T15N,R9W,Sec 4	32			Greene		Water		No
40		115725	39.821959	-90.097446	T16N,R9W,Sec 22	18			K Brown		Water		No
41		115726	39.821959	-90.097446	T16N,R9W,Sec 22	30			E C Trotter		Water		No
52		115640	39.836203	-90.022343	T16N,R8W,Sec 17	25			J H Hubbs		Water		No
53		115641	39.83617	-90.041154	T16N,R8W,Sec 18	32		1850	H Robinson		Water		No
54		115643	39.821671	-90.022214	T16N,R8W,Sec 20	26		1900	S Weinfeldt		Water		No
55		115644	39.821671	-90.022214	T16N,R8W,Sec 20	30		1904	Robinson		Water		No
56		115649	39.807149	-90.022402	T16N,R8W,Sec 29	26			M Walbaum		Water		No
57		115653	39.793	-90.022	T16N,R8W,Sec 32	18			Beggs		Water		No
58	121372070800	116522	39.77156	-90.0878	T15N,R9W,Sec 3	50		19770320	Linebarger, David		Water		No
59	121372118300	116520	39.769673	-90.080523	T15N,R9W,Sec 3	42			Harris, Frank R.		Water	Private Water Well	No
60	121372070700	116521	39.769673	-90.080523	T15N,R9W,Sec 3	40			harris F R		Water		No
61		116458	39.777	-90.126	T15N,R9W,Sec 5	30			Gary S. B.		Water		No
62		116464	39.761	-90.126	T15N,R9W,Sec 8	30			Cleray W		Water		No
63		116465	39.761	-90.126	T15N,R9W,Sec 8	40			Coons A		Water		No
64		116466	39.761	-90.107	T15N,R9W,Sec 9	30			Wallbaum W M		Water		No
65		116467	39.761	-90.107	T15N,R9W,Sec 9	35			Trotter l B		Water		No
66		227314	39.761	-90.107	T15N,R9W,Sec 9	40			Carl Shinnall #1		Water		No
67		116468	39.761	-90.089	T15N,R9W,Sec 10	30			Orear R		Water		No
68	121372070900	116525	39.765755	-90.080645	T15N,R9W,Sec 10	40			Linebarger D		Water		No
69		116469	39.761	-90.07	T15N,R9W,Sec 11	30			Collins W		Water		No
70		116470	39.761	-90.07	T15N,R9W,Sec 11	32			Lockhart G		Water		No
71		116393	39.776799	-90.032936	T15N,R8W,Sec 6	25		1923			Water		No
72		116394	39.776799	-90.032936	T15N,R8W,Sec 6	28			C Smith		Water		No
73	121372116800	116436	39.784526	-90.041604	T15N,R8W,Sec 6	54		19770226	Becker, Carl J.	1	Water	Livestock Watering Well	No
74	121372116900	116435	39.784526	-90.041604	T15N,R8W,Sec 6	43		19781010	Becker, Carl J.	1	Water	Private Water Well	No
75	121372117000	116434	39.782453	-90.041567	T15N,R8W,Sec 6	27		19761213	Smith, Lloyd E.	1	Water	Livestock Watering Well	No
76	121372161900		39.766277	-90.041266	T15N,R8W,Sec 7	26			Walpole, Ron		Water		No
77		116395	39.763	-90.033	T15N,R8W,Sec 7	30					Water		No
78		115696	39.836221	-90.059875	T16N,R9W,Sec 13	25			V R Mc Clure		Water		No

Map ID	API Number	ISWS ID	Latitude (NAD 83)	Longitude (NAD 83)	Public Land Survey System (PLSS)	Total Depth (ft)	Elevation (ft)	Completion Date	Owner	Well #	Well Type	Status	Confining Zone Penetration Well
79		115697	39.836221	-90.059875	T16N,R9W,Sec 13	27			U B Fox		Water		No
80		115698	39.836221	-90.059875	T16N,R9W,Sec 13	27			G W Lewis		Water		No
81		115699	39.836362	-90.078662	T16N,R9W,Sec 14	30			J Parrat		Water		No
82		115700	39.836362	-90.078662	T16N,R9W,Sec 14	28			C W Lewis		Water		No
83		115701	39.836362	-90.078662	T16N,R9W,Sec 14	28			J W Parrat		Water		No
84		115702	39.836362	-90.078662	T16N,R9W,Sec 14	32			J Hodgeson		Water		No
85	121372203900	356742	39.830101	-90.102984	T16N,R9W,Sec 15	47		20030910	Lomar Hager Construction		Water	Private Water Well	No
86		115703	39.836486	-90.097369	T16N,R9W,Sec 15	24			G Noulty		Water		No
87		115704	39.836486	-90.097369	T16N,R9W,Sec 15	30			L Lamkaular		Water		No
88		115705	39.836486	-90.097369	T16N,R9W,Sec 15	35			E E Hart		Water		No
89		115706	39.8365	-90.116151	T16N,R9W,Sec 16	23			S Jumper		Water		No
90		115707	39.8365	-90.116151	T16N,R9W,Sec 16	25			H Wester		Water		No
91		115722	39.821967	-90.116263	T16N,R9W,Sec 21	30			T J Ward		Water		No
92		115724	39.821967	-90.116263	T16N,R9W,Sec 21	30			C Trotter		Water		No
93		216249	39.821967	-90.116263	T16N,R9W,Sec 21	28		1934	Wm Noulty		Water		No
94	121370028400		39.822767	-90.073164	T16N,R9W,Sec 23	405		19540301	Keltner	1	Water		No
95	121372155100	237377	39.820978	-90.077895	T16N,R9W,Sec 23	42		19920414	Allen, John D.	1	Water	Private Water Well	No
96	121372207600	365042	39.822764	-90.075515	T16N,R9W,Sec 23	46		20040715	Burton, Larry		Water	Private Water Well	No
97	121372128400	115776	39.826288	-90.058992	T16N,R9W,Sec 24	40		19760220	Robinson, Leroy A.	1	Water	Private Water Well	No
98	121372128500	115777	39.828869	-90.059535	T16N,R9W,Sec 24	37		19781214	Romine, Buddy	1	Water	Private Water Well	No
99	121372211600	420169	39.813876	-90.103667	T16N,R9W,Sec 27	35		20060809	Donnan, Jeff		Water	Private Water Well	No
100		115744	39.807541	-90.116512	T16N,R9W,Sec 28	110			Noah B Fox		Water		No
101		115745	39.807541	-90.116512	T16N,R9W,Sec 28	28			Noah B Fox		Water		No
102		115746	39.807541	-90.116512	T16N,R9W,Sec 28	30			C Holdbrook		Water		No
103		115723	39.807541	-90.116512	T16N,R9W,Sec 28	28			W Noulty		Water		No
104	121372203000	348692	39.806645	-90.122622	T16N,R9W,Sec 28	42			Kendra Swain		Water		No
105		115759	39.792956	-90.116724	T16N,R9W,Sec 33	30			H Swain		Water		No
106		115760	39.792956	-90.116724	T16N,R9W,Sec 33	28			L L Hart		Water		No
107	121372155000		39.822856	-90.119949	T16N,R9W,Sec 21				Spradlin, Jack		Water		No
108	121370011400		39.833775	-90.10777	T16N,R9W,Sec 16	385	616	19551101	Wolfe, Eliz	1	Oil & Gas	Dry and Abandoned, No Shows, Plugged	No
109	121370011500		39.80091	-90.040421	T16N,R8W,Sec 30	420	635	19560101	Beilschmidt	1	Oil & Gas	Dry and Abandoned, No Shows, Plugged	No
110	121370011600		39.815108	-90.028322	T16N,R8W,Sec 20	365	610	19551201	Robinson, Howard	1	Oil & Gas	Dry and Abandoned, No Shows, Plugged	No
111	121370018900		39.825408	-90.062536	T16N,R9W,Sec 24	200		19440101	Lewis, E. C.		Oil & Gas	Dry Hole	No
112	121370024100		39.769077	-90.111454	T15N,R9W,Sec 4	580			Rayborn	1	Oil & Gas	Gas Producer	No
113	121370044200		39.770193	-90.110273	T15N,R9W,Sec 4	350			Rayburn	1	Oil & Gas	Gas Producer	No
114	121372086900		39.769679	-90.098565	T15N,R9W,Sec 4	301					Coal Test		No
115	121370024200		39.778927	-90.119618	T15N,R9W,Sec 5	423			Green, Laura & Effie	1	Oil & Gas	Gas Producer	No
116	121370024600		39.764523	-90.098492	T15N,R9W,Sec 9	293			Baxter	2	Oil & Gas	Dry and Abandoned, Gas Shows	No
117	121372094800		39.767065	-90.11144	T15N,R9W,Sec 9	325			Beilschmidt	1	Oil&Gas	Temporarily Abandoned	No
118	121372105200		39.763524	-90.104346	T15N,R9W,Sec 9				Leinberger	2	Oil&Gas	Permit to Drill Issued	No
119	121370007900		39.766464	-90.091366	T15N,R9W,Sec 10	295			Dunlap	8	Oil & Gas	Gas Producer	No
120	121372084800		39.766422	-90.065678	T15N,R9W,Sec 11	243					Coal Test		No
121	121370030900		39.806625	-90.105838	T16N,R9W,Sec 27	324	610	19591001	Fox, Lyman	1	Oil & Gas	Dry and Abandoned, No Shows, Plugged	No
122	121370033200		39.788212	-90.03349	T16N,R8W,Sec 31	323	641	19271001	Corrington	1	Oil & Gas	Dry and Abandoned, No Shows	No

Map ID	API Number	ISWS ID	Latitude (NAD 83)	Longitude (NAD 83)	Public Land Survey System (PLSS)	Total Depth (ft)	Elevation (ft)	Completion Date	Owner	Well #	Well Type	Status	Confining Zone Penetration Well
123	121370062300		39.828772	-90.06935	T16N,R9W,Sec 24	814	624	19700701	#MA-3		Stratigraphic or Structure Test	Structure Test, Plugged	No
124	121372068000		39.792709	-90.039363	T16N,R8W,Sec 31	142	641	19700518	Flynn, Robert		Coal Test		No
125	121372088400		39.829096	-90.098826	T16N,R9W,Sec 22	318	621	0			Coal Test		No
126	121372088600		39.801122	-90.108499	T16N,R9W,Sec 28	301	621	0			Coal Test		No
127	121372067800		39.814431	-90.023514	T16N,R8W,Sec 20	130	610	19700507	Newberry, Lucille		Coal Test		No
128	121372086000		39.83138	-90.055009	T16N,R9W,Sec 13	301	619	0			Coal Test		No

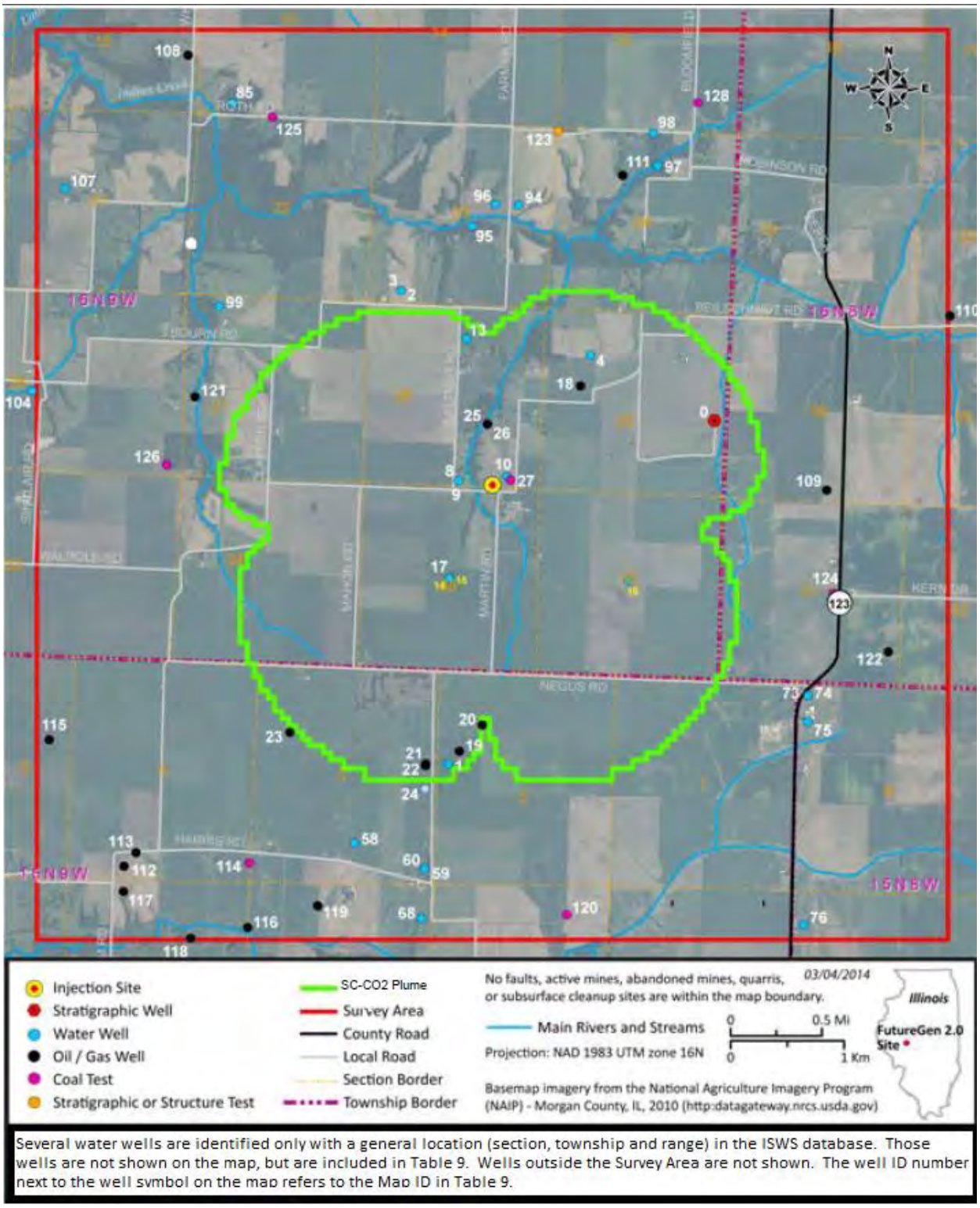

Figure 12. Wells Located Within the Survey Area

Proposed Operating Data (Operational Information)

Figure 13 and Figure 14 show the well design for the representative case for the refined area of the model domain in plan view, in 3D view, and in cross section view, respectively. Injection into four lateral wells with a well-bore radius of 4.5 in. was modeled with the lateral leg of each well located within the best layer of the injection zone to maximize injectivity. Only the non-cased open sections of the wells are specified in the model input file because only those sections are delivering CO_2 to the formation. The well design modeled in this case is the open borehole design [6], therefore part of the curved portion of each well is open and thereby represented in the model in addition to the lateral legs. The orientation and lateral length of the wells, as well as CO_2 mass injection rates, were chosen so that the resulting modeled CO_2 plume would avoid sensitive areas. The coordinates of the screened portion of the injection wells are shown in Table 10. The injection rate was assigned to each well according to the values in Table 11 for a total injection rate of 1.1 MMT/yr for 20 years. A maximum injection pressure of 2,252.3 psi (2,237.6 psig) was assigned at the top of the open interval (depth of 3,850 ft bgs or an elevation of -3,220 ft), based on 90 percent of the fracture gradient described in Section 3.5 (0.65 psi/ft).

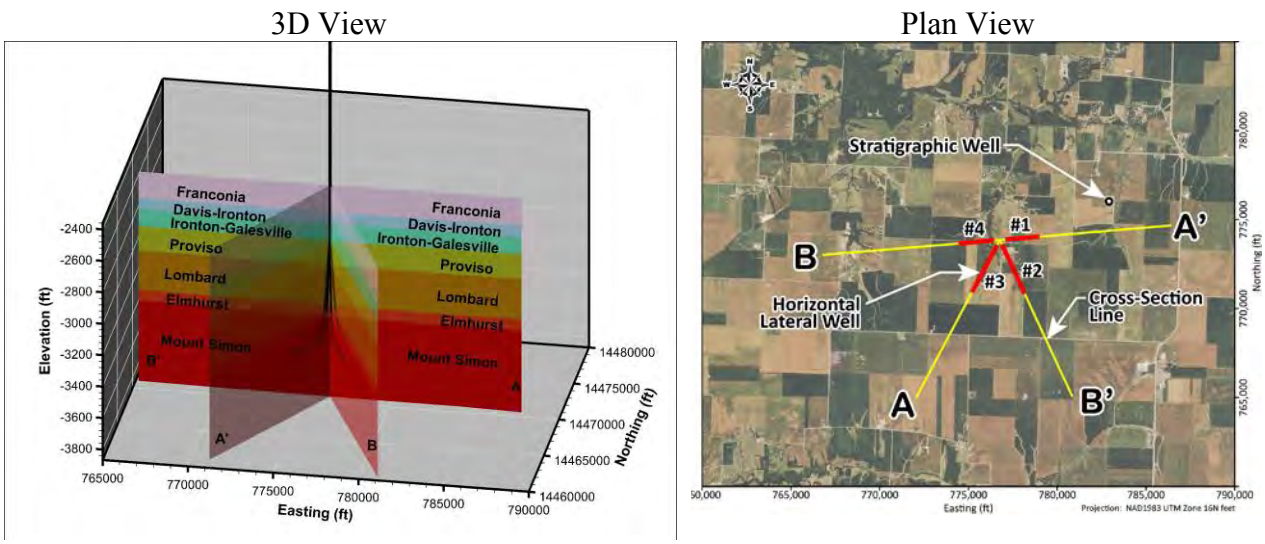

Figure 13. Operational Well Design for Representative Case Scenario as Implemented in the Numerical Model (with lateral legs of the injection wells shown in red and the cross section lines shown in yellow)

[6] Despite the models use of an open-hole design, the actual proposed construction is a cased hole with perforations.

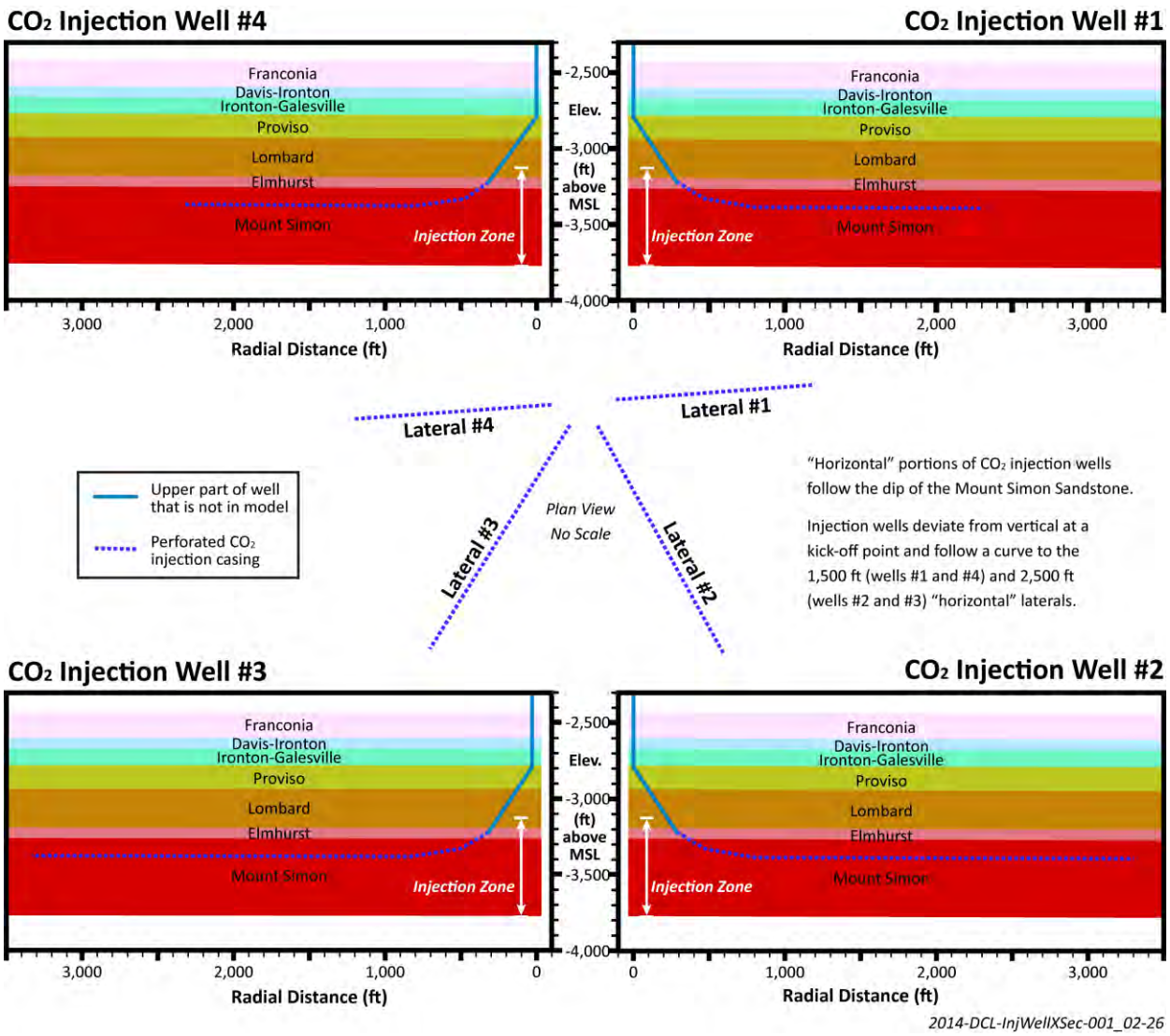

Figure 14. Cross Sections of CO_2 Injection Wells

Table 10. Coordinates (NAD1983 UTM Zone 16N) of Open Portions of the Injection Wells

	Coordinate 1(ft)			Coordinate 2(ft)			Coordinate 3(ft)			Coordinate 4(ft)		
	x	y	z	x	y	z	x	y	z	x	y	z
Well1	777079	14468885	-3220	777263	14468901	-3330	777592	14468929	-3387	779086	14469060	-3394
Well2	776898	14468571	-3220	776976	14468404	-3330	777116	14468105	-3388	778172	14465839	-3396
Well3	776617	14468578	-3220	776530	14468416	-3330	776375	14468124	-3382	775202	14465917	-3377
Well4	776451	14468829	-3220	776267	14468813	-3330	775938	14468785	-3377	774444	14468654	-3368

Table 11. Mass Rate of CO_2 Injection for Each of the Four Lateral Injection Wells

Well	Length of Lateral leg (ft)	Mass Rate of CO_2 Injection (MMT/yr)
Injection well #1	1,500	0.2063
Injection well #2	2,500	0.3541
Injection well #3	2,500	0.3541
Injection well #4	1,500	0.1856

Computational Modeling Results

At the end of the simulation period, 100 years, most of the CO_2 mass occurs in the CO_2 -rich (or separate) phase, with 20 percent occurring in the dissolved phase. Note that residual trapping begins to take place once injection ceases, resulting in about 15 percent of the total CO_2 mass being immobile at the end of 100 years. The CO_2 plume forms a cloverleaf pattern as a result of the four lateral injection-well design. The plume grows both laterally and vertically as injection continues. Most of the CO_2 resides in the Mount Simon Sandstone. A small amount of CO_2 enters into the Elmhurst and the lower part of the Lombard. When injection ceases at 20 years, the lateral growth becomes negligible but the plume continues to move slowly, primarily upward. Once CO_2 reaches the low-permeability zone in the upper Mount Simon it begins to move laterally. There is no CO_2 entering the confining zone. The maximum extent of the CO_2 plume, at 22 years, is in the center of Figure 15.

Pressure Front Delineation

As shown in Figure 16, the calculated hydraulic heads from the pressures and fluid densities measured in the Mount Simon Sandstone during drilling of the stratigraphic well range from 47.8 to 61.6 ft higher than the calculated hydraulic head in the lowermost USDW (St. Peter Sandstone). Based on these measurements, it was expected that the equation 1 suggested in the EPA AoR Guidance document (EPA 2013) for determination of the pressure front AoR would not be applicable for the FutureGen 2.0 Site since it would be in the “over-pressured” category. Thus alternative methods for assessment of the impacts of the pressure front would be needed for the “over-pressured” case at the FutureGen 2.0 Site.

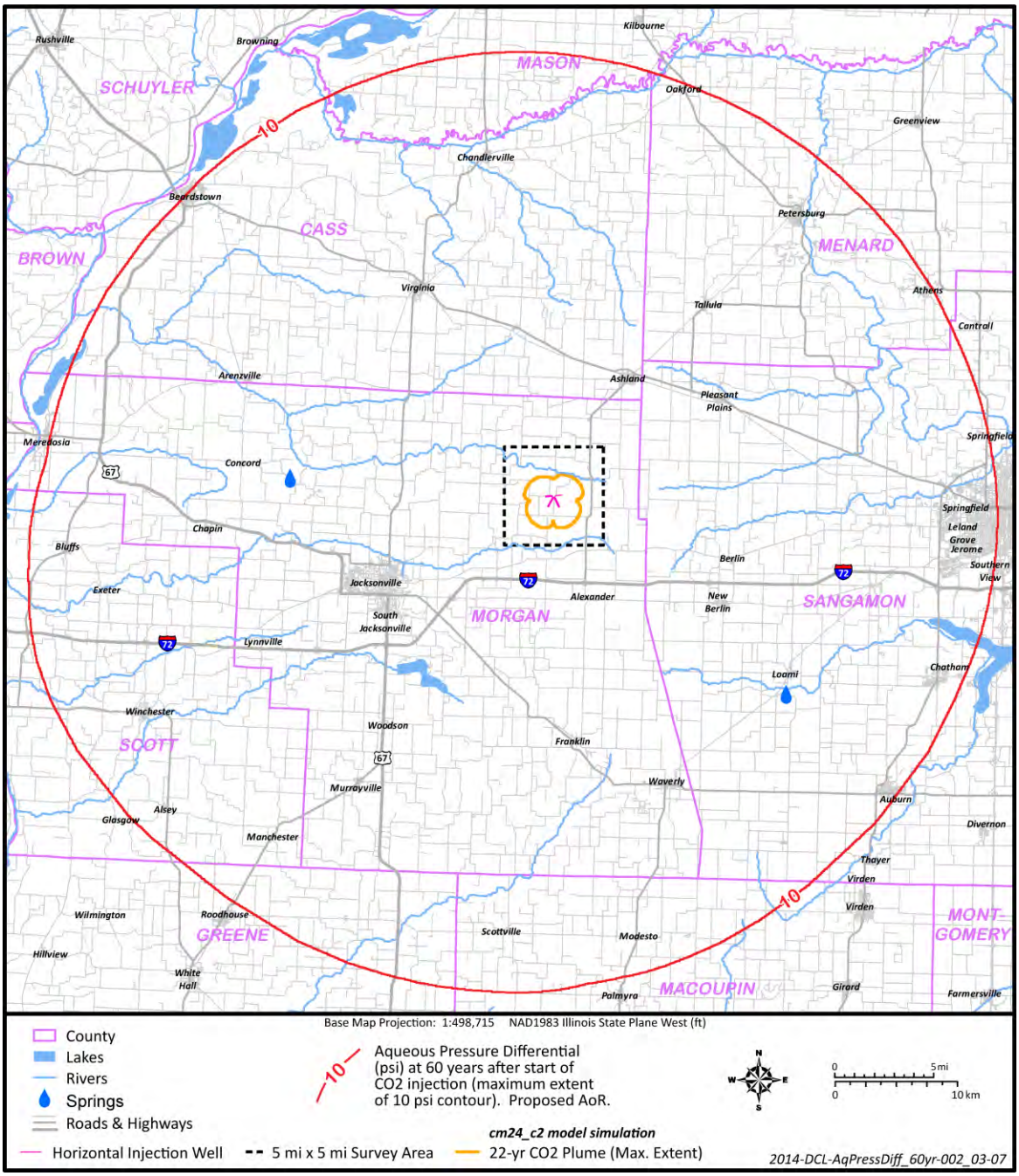

Figure 15. FutureGen Area of Review inclusive of the CO_2 plume and the area of elevated pressure delineated as the 10 psi contour at 60 years

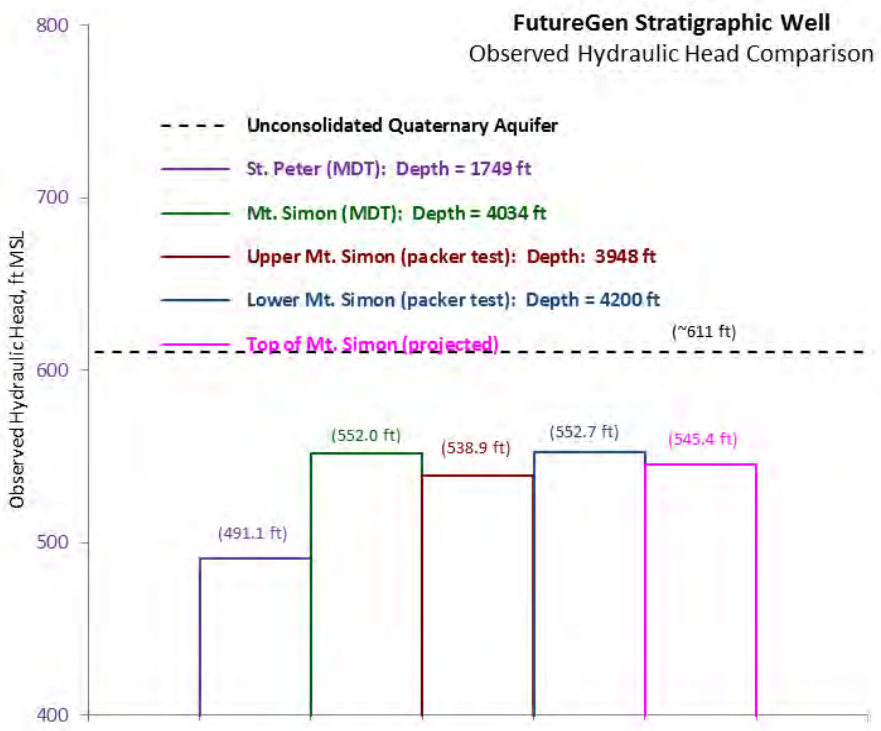

Figure 16. Observed Hydraulic Head Comparison between the Unconsolidated Quaternary Aquifer, St. Peter Sandstone, and Mount Simon Sandstone within the FutureGen Stratigraphic Well

Alternative approaches considered for delineation of an AoR inclusive of an area of elevated pressure

The FutureGen Alliance considered the applicability of and evaluated the project using an analytical solution (Cihan et al., 2011; 2013) and a range of other approaches (Table 13). The objective of these analyses was to assess, calculate, and account for critical pressure, which is the pressure great enough to mobilize fluids up an open conduit (i.e., an artificial penetration, fault, or fracture) from the injection zone into the overlying USDW. Methods evaluated are presented in Table 13.

Table 13. Methods Evaluated for Pressure Front Delineation

Approach	Results
AoR Guidance Equation 1	Not applicable
Nicot (2008)	13.76 psi
Birkholzer (2011)	9.65 psi
Cihan (2011): Assuming thief zones	Plume-sized AoR
Cihan (2011) Conservative: Assuming no thief zones	Large AoR

Pressure delineated AoR

Each of the pressure front analysis methodologies evaluated by the FutureGen Alliance (Table 13) are mathematical approximations applicable under prescribed conditions and subjected to simplifying assumptions. The simplified critical pressure calculations based on the open conduit concept are not applicable under site conditions because the ambient conditions in the lowermost USDW at the FutureGen site are under-pressured relative to the reservoir. Although the open conduit approaches are not strictly applicable under FutureGen site conditions, results from these conservative and protective approaches were used by EPA to delineate the pressure front AoR as the maximum extent of the 10 psi contour *of pressure differential* during the life of the project, which occurs 60 years after injection commences and is shown in Figure 15.

Corrective Action Plan and Schedule

No wells have been identified within the AoR that require corrective action.

Area of Review Reevaluation Plan and Schedule

Reevaluation Cycle

The FutureGen Alliance will reevaluate the AoR on an annual basis for the first 5 years following the initiation of injection operations (Figure 17). After the fifth year of injection, the AoR will be updated at a minimum of every 5 years as required by 40 CFR 146.84(b)(2)(i). An annual reevaluation in the first 5 years is intended to account for any operational variation during the startup period.

Some conditions will warrant reevaluation prior to the next scheduled cycle. To meet the intent of the regulations and protect USDWs, the following six conditions will warrant reevaluation of the AoR:

1. **Exceeding Fracture Pressure Conditions:** Pressure in any of the injection or monitoring wells exceeding 90 percent of the geologic formation fracture pressure at the point of measurement. This would be a violation of the permit conditions. The Testing and Monitoring Plan provides discussion of pressure monitoring.

   Action: The computational model will be calibrated to match measured pressures. Model outputs that calculate the change in AoR will be provided to EPA.

2. **Exceeding Established Baseline Hydrochemical/Physical Parameter Patterns:** A statistically significant difference between observed and baseline hydrochemical/physical parameter patterns (e.g., fluid conductivity, pressure, temperature) within the Ironton Formation immediately above the confining zone (ACZ1 and ACZ2 wells). The Student's t-test statistical procedure will be used to compare background (baseline) with observed

results. The Testing and Monitoring Plan provides extended information regarding how pressure, temperature, and fluid conductivity will be monitored within the Ironton Formation.

Action: In the event that hydrochemical/physical parameter trends suggest that leakage may be occurring, either the computational model or other models will be used to understand the observational parameter behavior.

3. **Compromise in Injection Well Mechanical Integrity:** A significant change in pressure within the protective annular pressurization system surrounding each injection well that indicates a loss of mechanical integrity at an injection well.

   Action: Injection wells suspected of mechanical integrity issues will be shut down and the cause of the pressure deviation determined. Mechanical integrity testing will be conducted and the computational model will be updated with mechanical integrity results to determine the severity and extent of the loss of containment. The Testing and Monitoring Plan provides extended information about the mechanical integrity tests that will be conducted in the injection wells.

4. **Departure in Anticipated Surface Deformation Conditions:** Surface deformation measurements that indicate an asymmetric or otherwise heterogeneous evolution of the injection zone pressure front, resulting in larger than predicted surface deformation outside the CO_2 plume. Areal surface deformation will be monitored using several technologies including differential synthetic aperture radar interferometry (DInSAR), which is a radar-based method that can measure very small changes in ground-surface elevation linked to pressure variations at depth. The area surveyed will extend beyond the predicted maximum extent of the CO_2 plume. If a measurable rise in the ground surface occurs outside the predicted extent, the AoR will be re-evaluated. The Testing and Monitoring Plan provides extended information about surface deformation monitoring.

   Action: The computational model will be calibrated to match observed pressures if they vary from the predicted deformation/pressure calculations.

5. **Seismic Monitoring Identification of Subsurface Structural Features:** Seismic monitoring data indicate the possible presence of a fault or fracture near the CO_2 injection zone in the sedimentary cover or in the basement (concentration of microearthquakes of $M<<1$ in elongated clusters). The Testing and Monitoring Plan provides extended information about the microseismic monitoring network.

   Action: The cause of the indicated microseismicity patterns will be evaluated. In conjunction, various operational parameters will be tested using the computational model to determine if the microseismic activity can be controlled to acceptable levels

6. **Seismic Monitoring Identification of Unexpected Plume Pattern:** Seismic monitoring data indicate a CO_2 plume migration outside the predicted extent. The observation of microearthquakes ($M<<1$) may also help define the actual shape of the maximum pressure field associated with the plume extensions.

Action: The computational model will be calibrated to match the location of observed microseismicity patterns indicative of plume extensions.

7. **Other triggers for reevaluation may include:** facility operating changes; new injection activities or other deep wells added in the AoR; new owner/operators; new site characterization data; a seismic event or other emergency; and unexpected changes in rate, direction, and extent of plume/pressure front movement.

Reevaluation Strategy

If any of these conditions occurs, the FutureGen Alliance will reevaluate the AoR to comply with requirements at 40 CFR 146.84 as described below. Ongoing direct and indirect monitoring data, which provide relevant information for understanding the development and evolution of the CO_2 plume, will be used to support reevaluation of the AoR. These data include: 1) the chemical and physical characteristics of the CO_2 injection stream based on sampling and analysis; 2) continuous monitoring of injection mass flow rate, pressure, temperature, and fluid volume; 3) measurements of pressure response at all site monitoring wells; and 4) CO_2 arrival and transport response at all site monitoring wells based on direct aqueous measurements and selected indirect monitoring method(s). The FutureGen Alliance will compare these observational data with predicted responses from the computational model and if significant discrepancies between the observed and predicted responses exist, the monitoring data will be used to recalibrate the model (Figure 17). In cases where the observed monitoring data agree with model predictions, an AoR reevaluation will consist of a demonstration that monitoring data are consistent with modeled predictions. As additional characterization data are collected, the site conceptual model will be revised and the modeling steps described above will be repeated to incorporate new knowledge about the site.

The FutureGen Alliance will submit a report notifying the UIC Program Director of the results of this reevaluation within 90 days of detection. At that time, the FutureGen Alliance will either: 1) submit the monitoring data and modeling results to demonstrate that no adjustment to the AoR is required; or 2) modify its Corrective Action, Emergency and Remedial Response, and other plans to account for the revised AoR. All modeling inputs and data used to support AoR reevaluations will be retained by the FutureGen Alliance for the period of the project.

To the extent that the reevaluated AoR is different from the one identified in this supporting documentation, the FutureGen Alliance will identify all active and abandoned wells and underground mines that penetrate the confining zone (the Eau Claire Formation) in the reevaluated AoR and will perform corrective actions on those wells. As needed, the FutureGen Alliance will revise all other plans, such as the Emergency and Remedial Response Plan, to take into account the reevaluated AoR and will submit those plans to the UIC Program Director for review and approval.

Note that seismic events are covered under the Emergency and Remedial Response Plan. A tiered approach to responding to seismic events will be based on magnitude and location. A notification procedure is provided in that plan.

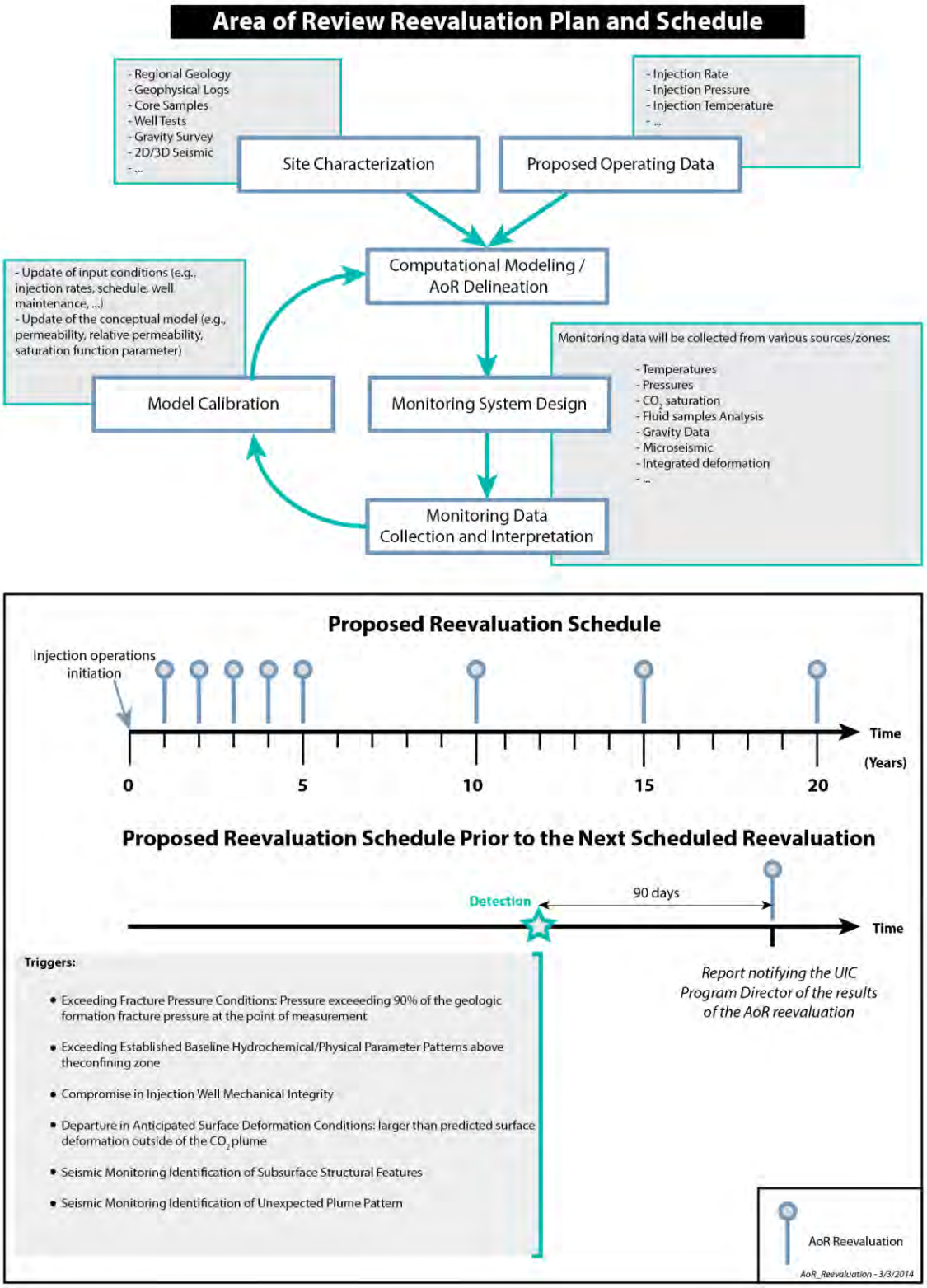

Figure 17. AoR Correction Action Plan Flowchart